CHALMERS
UNIVERSITY OF TECHNOLOGY

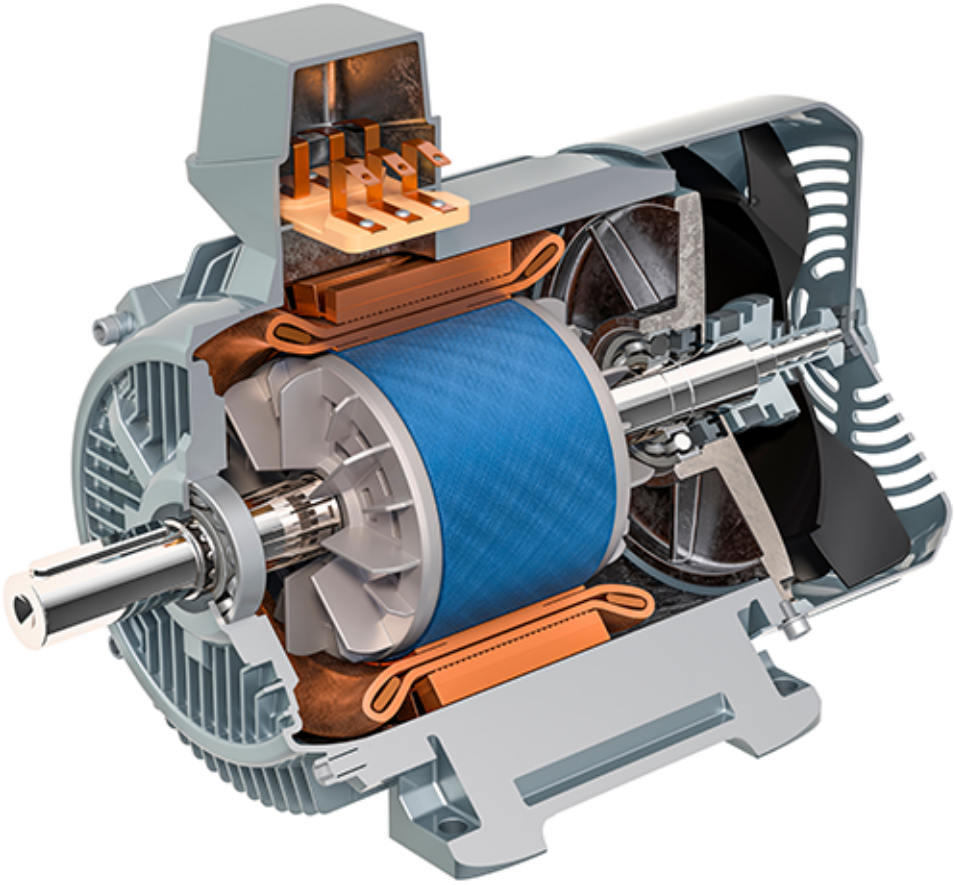

Rotor Resistance Estimation ASM

Master of Science Thesis

LANDER VALLEJO VARELA

Department of Electrical Engineering
Division of Electric Power Engineering
CHALMERS UNIVERSITY OF TECHNOLOGY
Gothenburg, Sweden 2023
www.chalmers.se

Master's thesis 2023

ROTOR RESISTANCE ESTIMATION ASM

LANDER VALLEJO VARELA

CHALMERS
UNIVERSITY OF TECHNOLOGY

Department of Electrical Engineering
Division of Electric Power Engineering
Chalmers University of Technology
Gothenburg, Sweden 2023

Comparison of rotor resistance estimator techniques for an induction machine.

LANDER VALLEJO VARELA

Supervisor: Johan Olsson, Volvo Cars Company
Examiner: Torbjörn Thiringer, Electrical Engineering Department

Master's Thesis 2023
Department of Electrical Engineering
Division of Electric Power Engineering
Chalmers University of Technology
SE-412 96 Gothenburg
Telephone +46 31 772 1000

Typeset in LaTeX
Printed by Chalmers Reproservice
Gothenburg, Sweden 2023

Rotor Resistance estimation ASM
LANDER VALLEJO VARELA
Department of Electrical Engineering
Division of Electric Power Engineering
Chalmers University of Technology

Abstract

Electric vehicles have experienced a surge in popularity in recent years due to the escalating global importance placed on sustainability. One of the key issues being addressed is the utilization of sustainable materials for electric motors. While certain electric vehicles employ permanent magnet synchronous machines (PMSMs) as their traction motors, these machines rely on rare earth materials. The process of mining rare earth materials is complex and has significant environmental impacts. Consequently, substantial efforts have been directed towards enhancing the performance of induction machines (IMs) to potentially replace PMSMs. A crucial aspect in achieving this goal is the accurate estimation of rotor resistance, which plays a vital role in narrowing the efficiency gap between IMs and PMSMs.

The main goal of this thesis was to compare different rotor resistance estimation techniques within a simulation environment. To achieve this, two distinct methods, deemed to be accurate, were tested. The software utilized throughout the thesis was MATLAB/SIMULINK. The first method employed a model reference adaptive system (MRAS), which involved comparing two models (reference and adaptive) to obtain the estimated rotor resistance. The second method relied on high frequency signal injection (HFSI), which affects the commanded reference torque, allowing for the estimation of the rotor resistance.

The simulation results obtained using MRAS and HFSI demonstrated successful estimation of the rotor resistance value, each with their respective advantages and disadvantages. One of the significant strengths of using reactive power MRAS is its independence from the stator resistance, which is a parameter subject to variation in real-life scenarios. On the other hand, HFSI offers a non-invasive and cost-effective approach, utilizing existing hardware for implementation. However, caution must be exercised regarding noise interference, as it has the potential to disrupt the frequency of the injected signal and lead to undesired machine behavior.

Keywords: IM, Rotor resistance, Sustainability, MRAS, HFSI

Acknowledgements

First and foremost, I would like to extend my utmost gratitude to my supervisors, Johan Olsson and Torbjörn Thiringer, for introducing me to the captivating world of motor control and for their guidance throughout this journey. I am sincerely thankful to Johan Zackrisson for placing his trust in me and providing the opportunity to work in such a dynamic and inspiring environment. Furthermore, I truly appreciate the consistent and motivating feedback you have graciously given me throughout the duration of this thesis.

I am also extremely grateful to the entire Machine Dynamics & Continuous Deployment department for their warm reception and support since the very beginning. A special mention goes to Joachim Härsjö. Thank you for attentively listening and being exceptionally patient with me during moments when I encountered difficulties in my thesis. Additionally, I would like to extend my thanks to Chalmers University for providing me with these amazing years of education.

To my friends, both those I had before coming to Sweden and those I have made since, thank you for everything we have shared and will continue to share together. I would also like to express my heartfelt appreciation to Maria, who has always stood by my side through thick and thin. I cannot emphasize enough how much I owe to your continuous support and help.

Finally, a special heartfelt thank you to my parents and my sister for their unwavering support and unconditional belief in me.

Lander Vallejo Varela, Gothenburg, June 2023

List of Acronyms

Below is the list of acronyms that have been used throughout this thesis listed in alphabetical order:

AC	Alternating Current
ASM	Asynchronous Machine
BPF	Band Pass Filter
CSI	Current Source Inverter
DC	Direct Current
DSP	Digital Signal Processor
EV	Electric Vehicle
HFSI	High Frequency Signal Injection
IFO	Indirect Field Orientation
IM	Induction Machine
LPF	Low Pass Filter
MRAS	Model Reference Adaptive System
MTPA	Maximum Torque Per Ampere
MTPV	Maximum Torque Per Voltage
PMSM	Permanent Magnet Synchronous Machine
PWM	Pulse Width Modulation
RFOC	Rotor Field Oriented Control
RPM	Revolutions Per Minute
VSI	Voltage Source Inverter

Nomenclature

Below is the nomenclature of parameters and variables that have been used throughout this thesis.

Variables

V_{sd}, V_{sq}	d-q components of the stator voltage vector.
i_{sd}, i_{sq}	d-q component of the stator current vector.
Ψ_{rd}, Ψ_{rq}	d-q component of the rotor flux vector.
R_s, R_r	Resistance of a stator and rotor phase winding.
L_s, L_r, L_m	Stator, rotor and mutual inductance.
L_{sl}, L_{rl}	Stator and rotor leakage inductance.
L_M, L_σ	Mutual and leakage inductance for inverse gamma model.
R_{ks}, R_R	Total and rotor resistance for inverse gamma model.
k	Transformation ratio for inverse gamma model.
Θ_m	Mechanical angle.
Θ_s	Stator electrical angle.
Θ_r	Rotor electrical angle.
w_m	Rotor speed in rad/s.
w_s	Synchronous angle in rad/s.
w_{sl}	Slip speed in rad/s.
n_p	Number of pole pairs.
n_s	Synchronous speed in RPM.
n_r	Rotor mechanical speed in RPM.
f_s, f_r	Synchronous and rotor's frequency.

Contents

1
Introduction

1.1 Problem background

Inverters are used in the automotive industry to be able to control electrical machines to produce the desired speed and torque to propel a vehicle. For induction machines (IM), also called asynchronous machines (ASM), both the magnetization level and the torque of the machine are controllable quantities. However, the fact that electrical machines are non-linear devices with time-varying parameters has motivated a lot of work in the control field during the last years [1], [2], [3], [4], [5], [6], [7]. To obtain an accurate machine controller it is important to have accurate estimations of the machine parameters at all operating points so that the controller can adapt the output to account for the current working conditions. Induction machines do not rely on rare earth materials. Therefore, with an accurate estimation of the rotor resistance, efficiency levels similar to those of permanent magnet synchronous machines (PMSMs) can be achieved, producing a positive social impact by reducing the use of rare earth materials. Consequently, electric cars may become more sustainable than combustion cars, consuming less energy for propulsion.

The transition towards decarbonization in various industries is gaining momentum, and one area of focus is the replacement of PMSMs with IM. This change holds significant potential for reducing carbon emissions and achieving sustainability goals.

Induction machines offer several advantages in the context of decarbonization. Firstly, they eliminate the need for rare earth magnets, which are typically used in PMSMs and have significant environmental and ethical concerns associated with their mining and extraction. By avoiding these magnets, the use of IMs helps to minimize the ecological footprint. Another advantage of induction machines is their compatibility with renewable energy sources. They can be seamlessly integrated into wind turbines, hydroelectric power plants, and other renewable energy systems, facilitating the expansion of clean energy generation and reducing dependence on fossil fuels.

The IM has a 3-phase winding connected to 3-phase balanced sinusoidal voltage supply (each phase displaced by 120 degrees) to produce a rotating flux. The 3-phase voltages will induce 3-phase balanced currents in the stator coils which, according to Ferrari's theorem, will generate a rotating magnetic field with constant magnitude [8]. The rotor, rotates at a slightly lower speed than the synchronous speed, and the difference between the synchronous and the actual rotor speed is called slip. The

slip is represented as a percentage or a fraction of the synchronous speed. Besides, the rotor in an IM does not have permanent magnets, instead, it has short circuited rotor bars. Due to the lack of permanent magnets in the rotor, the magnetic field in the rotor needs to be induced by the stator currents, causing new currents running in the rotor. These induced rotor currents interact with stator flux, and as a consequence, torque is generated. On the other hand, these currents also leads to resistance losses which heat up the rotor affecting the value of the resistance. It is well known in the literature that the rotor resistance may vary up to 100% of its nominal value due to rotor heating (see [1], [2]).

The Rotor Field Oriented Control (RFOC) is widely used in drive applications to guarantee a high-performance control [9], [10]. However, the feed-forward adjustment depends on rotor resistance value, which in case of not being properly estimated, will lead to inaccurate flux orientation, and as a consequence, the torque accuracy will be lost, leading to an unstable control system. Furthermore, the rotor resistance is an important parameter in determining the torque-speed characteristic of the motor [11]. For instance, if the estimated rotor resistance value is too high, the starting torque will be higher. Besides, the running slip will be high too, causing greater rotor copper losses and overheating. However, if the estimated rotor resistance is too low, the starting torque will be lower as seen in Figure 1.1.

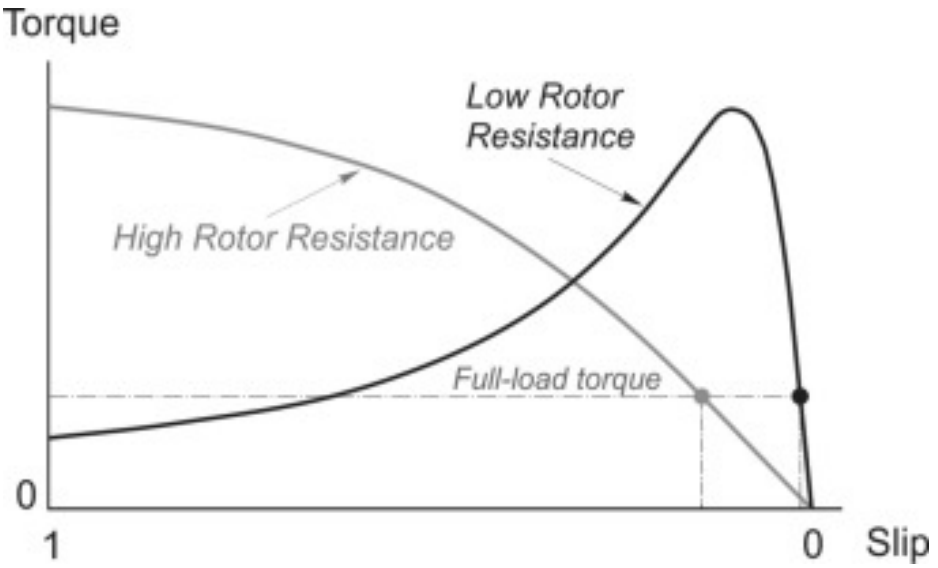

Figure 1.1: Torque variation with rotor resistance

Figure 1.1 shows how the torque varies related to the slip, the grey line represents the behaviour for a high rotor resistance and the black line for a low rotor resistance. It can be seen that when the IM is near to the working point (close to rated torque), the lower the rotor resistance, the steeper the slope of the torque, and thus, the slip will be smaller, reducing the rotor copper losses, and thereby, increasing the efficiency of the rotor which will be closer to the speed of synchronism.

In general, an accurate estimation of the rotor resistance is crucial for proper torque

control. If the machine is to be used in the automotive industry where there is a high demand on the torque accuracy, a good estimation of the rotor resistance must be obtained. An incorrect estimation can lead to an inaccurate rotor flux angle, resulting in the loss of torque control and an unstable system.

1.2 Previous work

During the last decades different methods such as signal injection [3], Model Reference Adaptive System (MRAS) [4]-[7] and observer-based [13] method among have been developed in control literature. Each method presents strengths and weaknesses, the observer-based method, for instance, needs a large memory requirement and computational intricacy. On the other hand, the signal injection model is computationally simpler, but there are adverse effects due to signal injection in motor dynamics. Regarding the MRAS, different quantities may be used for formulating the error including the electromagnetic torque, rotor flux and reactive power.

Not only these three methods have been developed, but also many other such as lumped-parameter thermal network [14], recursive least square [15], neural networks [16] or fuzzy logic [17]. However, there are not many direct comparisons between all of them.

1.3 Purpose

In a simulation environment develop a model of an IM and its controller which can be used to develop a method to accurately estimate the machine parameters with main focus on the rotor resistance. The aim is to evaluate different methods to estimate the parameters to investigate which provides the best results.

2

Theoretical Framework

2.1 Electromagnetism

Electromagnetism is the physical interaction among electric charges, magnetic moments, and the electromagnetic field [18]. The electromagnetic interaction is one of the four fundamental interactions of the physics. Magnetic and electric forces are found in magnetic and electric fields. All the electromagnetic effects arise from the interaction of electrically charged particles, particles with an intrinsic magnetic moment, and the electromagnetic field [18]. Electromagnetism is described by Maxwell's equations, which describe the behaviour of electric and magnetic fields by using the following differential equations

$$\Delta \times E = -\frac{\partial B}{\partial t} \tag{2.1}$$

$$\Delta \times H = J + \frac{\partial D}{\partial t} \tag{2.2}$$

$$\Delta \cdot E = \rho \tag{2.3}$$

$$\Delta \cdot B = 0 \tag{2.4}$$

where E is the electric field strength in $[V/m]$, B is the magnetic flux density in $[T]$, H is the magnetic field strength in $[A/m]$, J is the current density in $[A/m^2]$, D is the electric flux density in $[C/m^2]$ and ρ is electric charge density in $[C/m^2]$. Moreover, the properties of electromagnetic materials are

$$D = \varepsilon E \tag{2.5}$$

$$B = \mu H \tag{2.6}$$

$$J = \sigma E \tag{2.7}$$

where ε is the permittivity of the material in $[F/m]$, μ is the permeability in $[Vs/Am]$ and σ is the conductivity in $[S/m]$.

The basic magnetic circuit can be compared to the basic electric circuit as seen in Figure 2.1

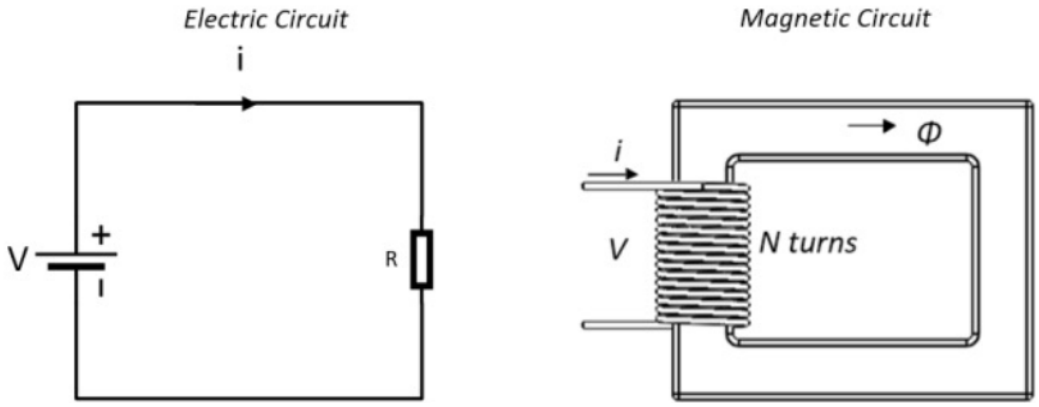

Figure 2.1: Magnetic and electric circuits

In the magnetic circuit, the equation that describes the behaviour of the circuit is

$$\mathcal{F} = \phi\mathcal{R} \tag{2.8}$$

where $\mathcal{F}$ is the magneto motive force (mmf) in $[A - turns]$, ϕ is the magnetic flux in $[Wb]$ and $\mathcal{R}$ is the reluctance in $[A - turns/Wb]$.

2.1.1 Ampère's Law

Ampère's law relates the formation of a resulting magnetic field when a continuous electric current is passing through the conductor of any shape [19]. The equation that governs this law can be expressed as

$$\oint B\,ds = \mu_0 I \tag{2.9}$$

where $\oint B$ is the line integral of the magnetic field, ds is any arbitrary closed path, μ_0 is the magnetic permeability of the vacuum, and I is the total current that is passing through any open surface bounded by the closed path. In other words, any time that a current flows through a conductor, a magnetic field which will circulate on a perpendicular plane to the conductor as Figure 2.2 depicts. The direction of the magnetic field will be given by the right hand rule.

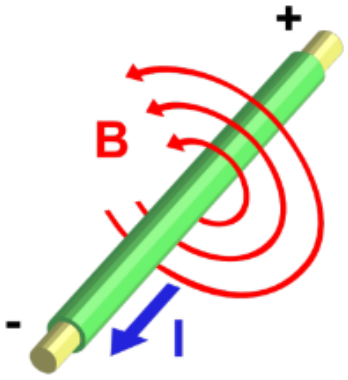

Figure 2.2: Current through conductor creating a magnetic field

2.1.2 Faraday's Law of Induction

Faraday's law of induction states how an electromotive force (emf) can be obtained due to the interaction of a magnetic field with an electric circuit. This phenomenon is known as electromagnetic induction. It is the fundamental operating principle of transformers, inductors, and many types of electric motors, generators and solenoids. It is well known that,

$$\phi = \int B\, dA \tag{2.10}$$

where ϕ is the magnetic flux. In general, the loop may have several turns, N. The flux linkage is obtained as

$$\Psi = N\phi \tag{2.11}$$

In general, the electromotive force can be created in two different ways. In the first case, the area is constant and the magnetic flux density changes, whereas in the second case, the magnetic flux density (B) is constant and the are varies. As a consequence, it is obtained that

$$\varepsilon = -\frac{d\phi}{dt} = -\frac{d(BA)}{dt} = -A\frac{dB}{dt} = -B\frac{dA}{dt} \tag{2.12}$$

Once more, if the loop has several turns, the electromotive force will be given as

$$\varepsilon = -N\frac{d\phi}{dt} = -\frac{d\Psi}{dt} \tag{2.13}$$

The negative sign comes from Lenz's law, which says that the induced current in a loop will oppose the change of the magnetic field [19].

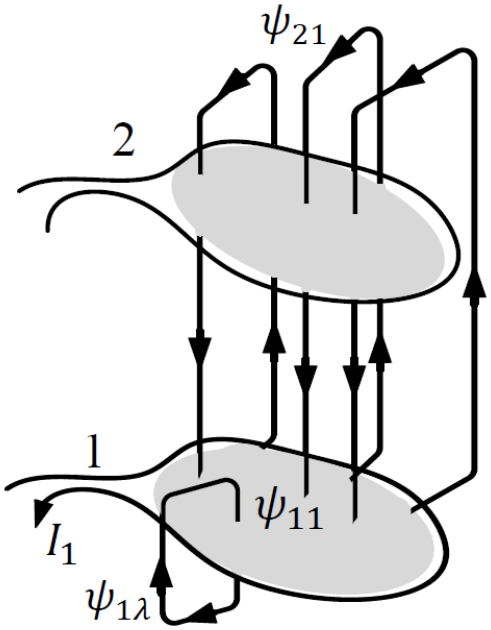

Figure 2.3: Flux linkage between two coils

The self flux linkage Ψ_{11} when running a current I_1 through coil 1 as shown in Figure 2.3 can be obtained as

$$\Psi_{11} = L_{11}I_1 \tag{2.14}$$

This is the total flux linkage created in coil 1 by the current I_{11}. The relation between the self flux linkage and the current is the self inductance L_{11}.

If a second coil is introduced, coil 2, as can be seen in Figure 2.3, the main part of the self flux linkage of coil 1 also links with coil 2, this part is called the mutual flux

$$\Psi_{21} = L_{21} I_1 \tag{2.15}$$

This is the flux linkage in coil 2 cause by I_1. The inductance L_{21} is the mutual inductance and the mutual inductance satisfies that $L_{21} = L_{12} = L_M$. This means that the magnetic connection between coil 1 and 2 is the same as the one between coil 2 and 1.

The part of the self flux linkage of coil 1 that does not link with coil 2 is

$$\Psi_{1\lambda} = L_{1\lambda} I_1 \tag{2.16}$$

This is called the leakage flux and the inductance is the leakage inductance. The total flux is calculated as,

$$\Psi_{11} = \Psi_{1\lambda} + \Psi_{21} \tag{2.17}$$

2.2 Clarke and Park Transformation

The Clarke and Park transformations are two mathematical methods used to transform three-phase electrical quantities into two-phase quantities. These transformations are commonly used in the analysis and control of three-phase systems, such as IM.

2.2.1 Clarke Transformation

The Clarke transformation converts the three-phase quantities (i.e., currents or voltages) into two-phase quantities, known as the alpha-beta components. The alpha-beta components are orthogonal to each other and are related to the three-phase quantities by the following equations

$$\begin{bmatrix} s_\alpha \\ s_\beta \end{bmatrix} = K \begin{bmatrix} \frac{2}{3} & -\frac{1}{3} & -\frac{1}{3} \\ 0 & \frac{1}{\sqrt{3}} & -\frac{1}{\sqrt{3}} \end{bmatrix} \begin{bmatrix} s_a \\ s_b \\ s_c \end{bmatrix} \tag{2.18}$$

where s_a, s_b and s_c are the three-phase quantities and K is the scaling constant. The scaling constant can be selected arbitrarily. During this thesis the amplitude invariant scaling will be used, in which $K = 1$.

The Clarke transformation is used to simplify the analysis and control of three-phase systems by reducing the complexity of the mathematical expressions involved. Moreover, if there is no zero-sequence (i.e. if all phase values added are equal to zero all the time), no information is lost when transforming from three-phase to two-phase. The alpha-beta reference frame is also called stationary reference frame.

2.2.2 Park Transformation

The Park transformation (also known as the dq transformation) converts the three-phase quantities into two-phase (d-q) quantities, which are orthogonal to each other and aligned with the rotor flux of an IM. The transformation involves two steps:

1. Clarke transformation is used to transform the three-phase quantities into the alpha-beta components.
2. The alpha-beta components are then transformed into the d-q components using the following equations

$$\begin{bmatrix} s_d \\ s_q \end{bmatrix} = \begin{bmatrix} \cos\Theta & \sin\Theta \\ -\sin\Theta & \cos\Theta \end{bmatrix} \begin{bmatrix} s_\alpha \\ s_\beta \end{bmatrix} \tag{2.19}$$

where Θ is the angle between the alpha-beta reference frame and the d-q reference frame.

The Park transformation is useful in the analysis and control of IM, where the d-axis represents the flux-producing component and the q-axis represents the torque-producing component. By transforming the three-phase currents and voltages into

the d-q components, it is possible to design and implement control strategies that decouple the control of the flux and torque, making it easier to regulate the machine performance.

In the dq-system the signals are observed in a system that rotates with the same speed as the machine, thereby signals are seen as stationary quantities, i.e a DC signal. However, in the alpha-beta system the quantities are observed in the stationary system (alpha-beta), then signals are seen as rotating quantities, i.e an AC signal.

2.3 Induction Machine

Induction machines are devices that convert electric energy into mechanical energy (motors), or vice versa (generators). All electric machines have two main parts that are clearly distinguished: stator and rotor.

The working principle of an IM is based on the interaction between magnetic fields, which will create an electromagnetic force that rotates a shaft obtaining a certain torque when a sinusoidal three phase voltage is supplied. When the voltage is supplied to the stator windings, a rotating magnetic field is produced which will rotate at a certain speed determined by the number of pole pairs and the frequency of the voltage. The aforementioned speed, is called synchronous speed and it is given by (2.20). The rotor of an IM can be either wound or squirrel cage (which has copper or aluminium rods embedded in slots, all short circuited together at each end). Besides, the rotor, rotates at a slightly lower speed than the synchronous speed. The difference in speed, induces voltages in the short circuited rotor bars, and therefore, rotor currents are generated.

$$n_s = 60\frac{f}{n_p} \tag{2.20}$$

where f is the frequency in $[Hz]$ and n_p is the number of pole pairs. As the number of pole pairs is decided in the design phase, the only way of controlling the synchronous speed of the machine is varying the frequency of the AC voltage. Squirrel cage rotor is the most common one due to the robustness and the very low maintenance that requires. Since the cage needs to be magnetized and the magnetization happens due to the offset in stator an rotor magnetic field, the rotor of an IM rotates at a slightly lower speed than the synchronous speed. The difference in speed, induces voltages in the short circuited rotor bars, therefore, rotor currents are generated. These induced rotor currents create their own magnetic field according to Ampere's law, which will interact with stator flux, and as a consequence, torque is generated. The slip of an IM is related to the rotor's mechanical and electrical characteristics such as load and rotor resistance, and it is calculated as

$$s = \frac{n_s - n_r}{n_s} \tag{2.21}$$

where n_r is the rotor mechanical speed in revolutions per minute (RPM). Once the

slip is known, the frequency of the rotor can be calculated as

$$f_r = sf_s \tag{2.22}$$

In Figure 2.4 an axial view of an IM is illustrated, where the main parts that compose the machine are distinguished.

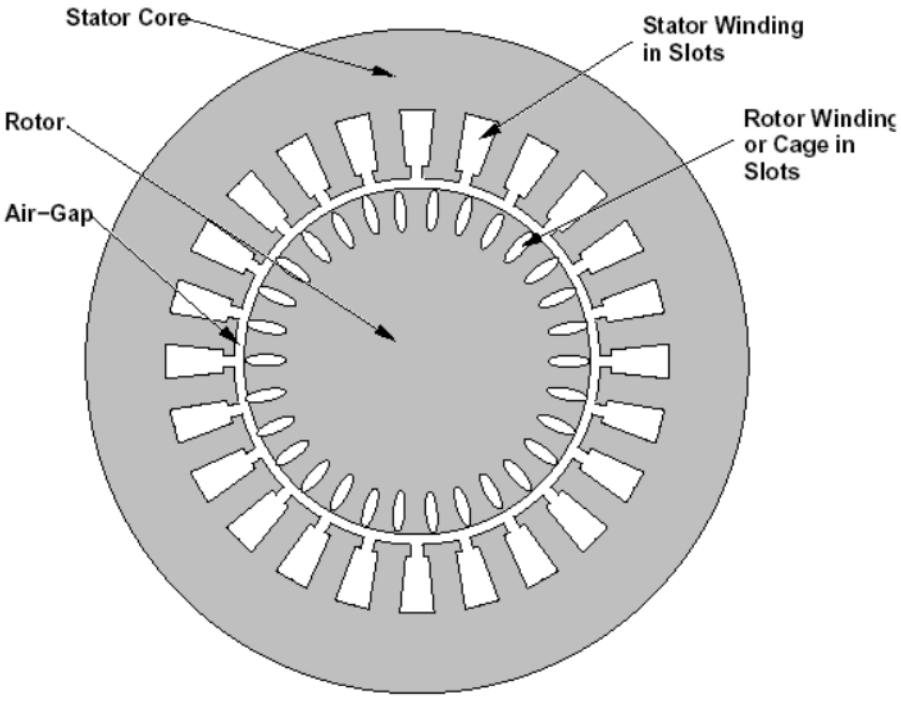

Figure 2.4: Axial view of an IM

2.3.1 Induction Machine Modeling

Consider a three-phase IM with 120 degrees winding displacement in both stator and rotor. In Figure 2.5 the magnetic axes are presented.

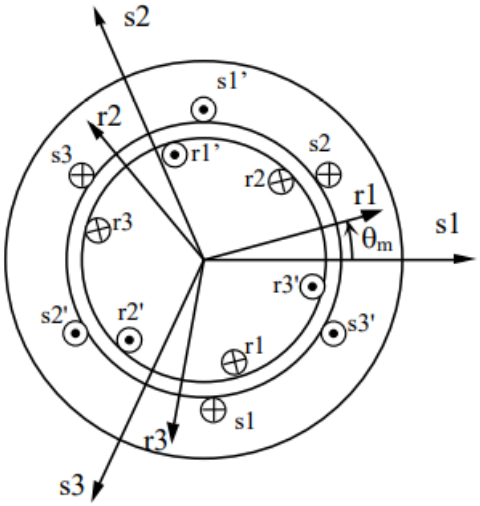

Figure 2.5: Induction machine structure

If the stator windings are supplied by a sinusoidal 3-phase system of voltages with 120° displacement, as seen in the classical theory, the three currents are equal in amplitude and with a displacement of 120 degrees (1/3 of the period). A rotating field, with a sinusoidal distribution along the air-gap, is generated according to Ferrari's theorem.

Suppose that the machine is rotating at a speed Ω_m; the behavior can be studied using the mutually coupled theory. This brings to a system of equations as

$$V_k = R_k i_k + \frac{d\Psi_k}{dt} \tag{2.23}$$

where k refers to one of the six windings (3 in the stator and 3 in the rotor), V_k is the voltage of the k-th winding, R_k is the resistance of the k-th winding and Ψ_k is the flux linked with the k-th winding.

We must then consider the relationship between fluxes and currents,

$$\Psi_k = \sum_i L_{ki}(\Theta_m) i_i \tag{2.24}$$

where the mutual inductance $L_{ki}(\Theta_m)$ is a function of the mechanical angle (Θ_m) between the magnetic axes of the rotor and the stator. The mechanical equation of the torque for an IM is given by

$$T_e - T_r = J\frac{d\Omega_m}{dt} + B\Omega_m \tag{2.25}$$

Now, consider a reference frame fixed with the stator (stationary frame) applying the space phasor formula to the three stator equations (Clarke transformation). The new machine model will only have two stator winding instead of three, fixed with the stator itself and orthogonal each other, crossed by two currents: the real and imaginary parts of the stator current space phasor. It results in

$$\vec{V}_s^s = R_s \vec{i}_s^s + \frac{d\vec{\Psi}_s^s}{dt} \tag{2.26}$$

Similarly, a reference frame fixed with the rotor may be consider for rotor quantities. Applying the space phasor formula to the rotor windings, two rotor winding will be obtained, fixed with the rotor and orthogonal with each other. It results in

$$\vec{V}_r^r = R_r \vec{i}_r^r + \frac{d\vec{\Psi}_r^r}{dt} \tag{2.27}$$

However, the chosen reference frames are not the same, so there is no way to compare stator an rotor quantities. This is why it is necessary to have a unique reference frame. Among all the possibilities, a reference frame fixed with the stator is chosen. Taking into account the space phasor formula, it is well known that the rotor quantities seen in a stator reference frame becomes

$$\vec{V}_r^s = R_r \vec{i}_r^s + \frac{d\vec{\Psi}_r^s}{dt} - jw_m \vec{\Psi}_r^s \tag{2.28}$$

The relation between fluxes and currents is expressed as

$$\vec{\Psi}_s^s = L_s \vec{i}_s^s + M \vec{i}_r^s \tag{2.29}$$

$$\vec{\Psi}_r^s = L_r \vec{i}_r^s + M \vec{i}_s^s \tag{2.30}$$

The model presented is called the 5 parameters dynamic model of the IM (R_s, R_r, L_s, L_r, M). The expression of the torque is obtained from the energy balance. The total input power is:

- Dissipated into heat by Joule effect.
- Used to change the magnetic energy stored in the self and mutual inductance.
- Transformed into mechanical power.

Therefore, once the mechanical power is known, the torque expression may be achieved as

$$T_e = \frac{P_m}{\Omega_m} \tag{2.31}$$

From energy balance it is achieved that the mechanical power is

$$P_m = \frac{3}{2} Re(-jw_m \vec{\Psi}_r^s \bar{i}_r^s) = \frac{3}{2} Im(w_m \vec{\Psi}_r^s \bar{i}_r^s) = \frac{3}{2} w_m Im(\vec{\Psi}_r^s \bar{i}_r^s) \tag{2.32}$$

And it is known that

$$w_m = n_p \Omega_m \tag{2.33}$$

As a result, the torque expression is given by

$$T_e = \frac{3}{2} n_p Im(\vec{\Psi}_r^s \bar{i}_r^s) \tag{2.34}$$

Using the relation between the flux and currents (Eq 2.29, 2.30) it is possible to obtain different expressions of the torque,

$$T_e = \frac{3}{2} n_p Im(\vec{\Psi}_r \bar{i_r}) = \frac{3}{2} n_p \frac{M}{L_r} Im(\vec{i_s} \bar{\Psi}_r) = \frac{3}{2} n_p Im(\vec{i_s} \bar{\Psi}_s) = \\ = \frac{3}{2} n_p \frac{M}{L_r(L_s - \frac{M^2}{L_r})} Im(\vec{\Psi}_s \bar{\Psi}_r) \tag{2.35}$$

Lets now consider a generic reference frame dq, rotated by Θ_s with respect to the stator, see Figure 2.6. The dynamic model of the IM in this new frame is

$$\vec{V_s} = R_s \vec{i_s} + \frac{d\vec{\Psi}_s}{dt} + jw_s \vec{\Psi}_s \tag{2.36}$$

$$\vec{V_r} = R_r \vec{i_r} + \frac{d\vec{\Psi}_r}{dt} + jw_{sl} \vec{\Psi}_r \tag{2.37}$$

$$T_e - T_r = J \frac{d\Omega_m}{dt} + B\Omega_m \tag{2.38}$$

with $\Theta_r = \Theta_s - \Theta_m$

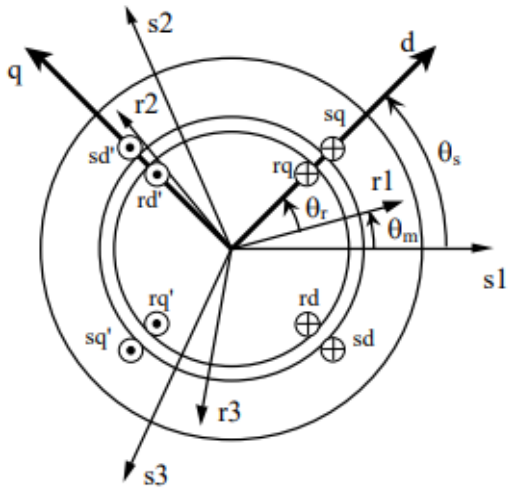

Figure 2.6: IM in the new d and q axes

Due to the use of the stator reference frame for rotor quantities, the dependence of the mutual inductance on the angle Θ_m is eliminated. By assuming that an ideal transformer with a transformation ratio k is connected to the rotor, the four parameter dynamic model may be derived. The rotor quantities will be linked to the original variables by the following relation

$$\frac{\vec{V_r}}{\vec{V_r'}} = \frac{\vec{\Psi}_r}{\vec{\Psi}_r'} = \frac{\vec{i_r'}}{\vec{i_r}} = \frac{1}{k} \tag{2.39}$$

In fact, if the transformation ratio is chosen so that $k = \frac{M}{L_r}$, the series inductance of the rotor side is cancelled. It is important to remember that not only the rotor

series inductance will be cancelled, but also the rotor resistance and the mutual and stator series inductance will change as

$$R_r^{'} = k^2 R_r \tag{2.40}$$

$$M^{'} = kM \tag{2.41}$$

$$L_{ks} = L_s - kM \tag{2.42}$$

The voltage $V_r^{'}$ is linked to the real voltage V_r, but since normally the rotor of an induction machine is short-circuited, this voltage is zero. On the other hand, the rotor current is not measurable in the case in which the rotor is constructed by a squirrel cage structure and therefore the transformation ratio k does not affect these parameters. From these considerations, it results that it is not necessary to know the transformation ratio k. It is important to remember that the introduction of an ideal transformer enables to introduce a degree of freedom, while maintaining the equivalence at the external terminals. This degree of freedom is used, in this case, to cancel the series inductance rotor side. From now on, the parameters that are in the left par of the transformer in Figure 2.7 will be noted as V_r instead of $V_r^{'}$ for simplicity. These changes will result in the four parameter equivalent circuit presented in Figure 2.7.

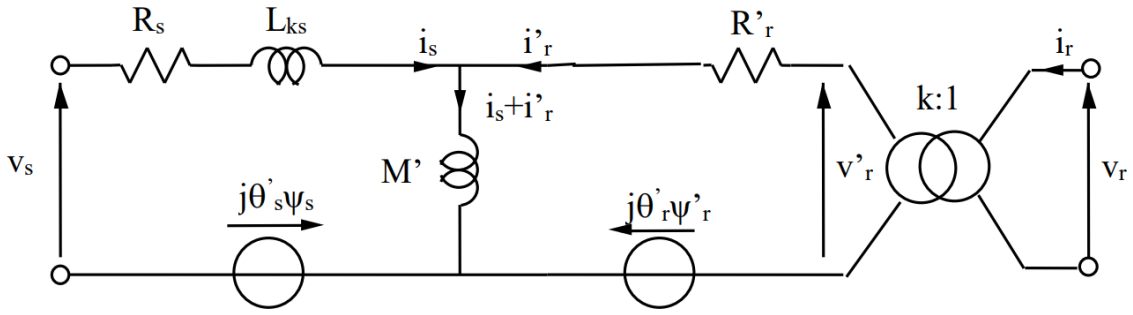

Figure 2.7: Four parameter equivalent circuit with a suitable k

The four parameters dynamic model of an IM becomes

$$\vec{V_s} = R_s \vec{i_s} + \frac{d\vec{\Psi}_s}{dt} + jw_s \vec{\Psi}_s \tag{2.43}$$

$$\vec{V_r^{'}} = R_r^{'} \vec{i_r^{'}} + \frac{d\vec{\Psi}_r^{'}}{dt} + jw_{sl} \vec{\Psi}_r^{'} \tag{2.44}$$

$$\vec{\Psi}_s = L_{ks} \vec{i_s} + M^{'}(\vec{i_s} + \vec{i_r^{'}}) = L_{ks} \vec{i_s} + \vec{\Psi}_r^{'} \tag{2.45}$$

$$\vec{\Psi}_r^{'} = M^{'}(\vec{i_s} + \vec{i_r^{'}}) \tag{2.46}$$

$$T_e - T_r = J\frac{d\Omega_m}{dt} + B\Omega_m \tag{2.47}$$

2.4 Vector Control of an Induction Machine

The vector control of an IM is based on a suitable choice of reference axis used by the controllers so that a component of the stator current space phasor acts only on the flux, while the other one acts on the electromagnetic torque.

To illustrate the principle of field-oriented control, the IM dynamic model has to be recalled. Lets consider the dynamic equations of the IM referred to a rotating dq reference frame

$$\vec{V_s} = R_s\vec{i_s} + \frac{d\vec{\Psi}_s}{dt} + jw_s\vec{\Psi}_s \tag{2.48}$$

$$\vec{V_r} = 0 = R_r\vec{i_r} + \frac{d\vec{\Psi}_r}{dt} + jw_{sl}\vec{\Psi}_r \tag{2.49}$$

$$T_e - T_r = J\frac{d\Omega_m}{dt} + B\Omega_m \tag{2.50}$$

There is also a relation between fluxes and currents

$$\vec{\Psi}_s = L_{ks}\vec{i_s} + \vec{\Psi}_r \tag{2.51}$$

$$\vec{\Psi}_r = L_M(\vec{i_s} + \vec{i_r}) \tag{2.52}$$

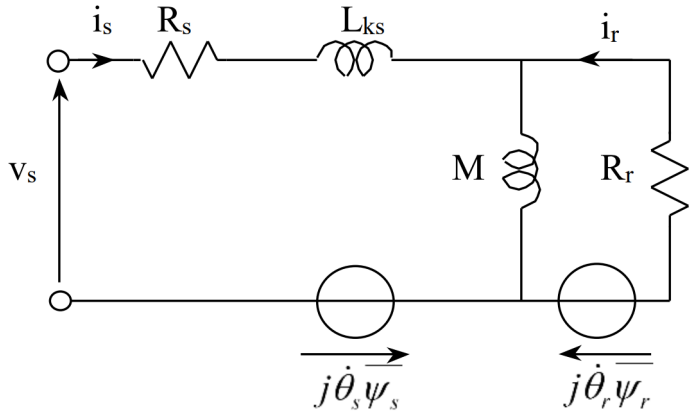

Figure 2.8: Dynamic equivalent circuit

From equation 2.52, the rotor current can be obtained as

$$\vec{i_r} = \frac{\vec{\Psi}_r}{L_M} - \vec{i_s} \tag{2.53}$$

Substituting the equations 2.51, 2.52 and 2.53 in the voltage ones (2.48 and 2.49), the system expressed in the electrical state variables i_s and Ψ_r is achieved

$$\vec{V_s} = R_s\vec{i_s} + L_{ks}\frac{d\vec{i_s}}{dt} + \frac{d\vec{\Psi}_r}{dt} + jw_sL_{ks}\vec{i_s} + jw_s\vec{\Psi}_r \tag{2.54}$$

$$0 = \frac{R_r}{L_M}\vec{\Psi}_r - R_r\vec{i_s} + \frac{d\vec{\Psi}_r}{dt} + jw_{sl}\vec{\Psi}_r \tag{2.55}$$

where the rotor voltages are zero, since it is an IM that has a short-circuit rotor. From the rotor voltage equation it results in

$$\frac{d\vec{\Psi}_r}{dt} = R_r\vec{i_s} - \frac{R_r}{L_M}\vec{\Psi}_r - jw_{sl}\vec{\Psi}_r \tag{2.56}$$

Substituting the obtained equation in the stator voltage equation and taking into account that $w_r = w_s - w_m$ and $R_{ks} = R_s + R_r$, it is derived that

$$\vec{V_s} = R_{ks}\vec{i_s} + L_{ks}\frac{d\vec{i_s}}{dt} - \frac{R_r}{L_M}\vec{\Psi}_r + jw_sL_{ks}\vec{i_s} + jw_m\vec{\psi_r} \tag{2.57}$$

Once again, substituting the fluxes and currents relation in the electromechanical torque expression, the torque is obtained as

$$T_e = \frac{3}{2}n_pIm(\vec{i_s}\bar{\Psi}_r) \tag{2.58}$$

At this point the d and q axes are chosen in such a way that the d-axis is perfectly oriented with the rotor flux space phasor. With this choice, the quadrature component of the rotor flux is always zero, so:

$$\Psi_{rd} = \Psi_r = L_M i_{sd} \qquad and \qquad \Psi_{rq} = 0$$

The resulting equations for the d and q axes become

$$V_{sd} = R_{ks}i_{sd} + L_{ks}\frac{di_{sd}}{dt} - \frac{R_r}{L_M}\Psi_r - w_sL_{ks}i_{sq} \tag{2.59}$$

$$V_{sq} = R_{ks}i_{sq} + L_{ks}\frac{di_{sq}}{dt} + w_m\Psi_r + w_sL_{ks}i_{sd} \tag{2.60}$$

$$\frac{d\Psi_r}{dt} = R_r i_{sd} - \frac{R_r}{L_M}\Psi_r \tag{2.61}$$

$$0 = R_r i_{sq} - w_{sl}\Psi_r \tag{2.62}$$

$$\frac{dw_m}{dt} = \frac{n_p(T_e - T_r) - Bw_m}{J} \tag{2.63}$$

$$T_e = \frac{3}{2}n_pL_M i_{sd}i_{sq} \tag{2.64}$$

where w_s and w_r mean respectively the speed of the reference frame (fixed with the rotor flux) respect to the stator and rotor windings.

The aforementioned set of equations expressed in canonical form become

$$\frac{di_{sd}}{dt} = \frac{1}{L_{ks}}[V_{sd} - R_{ks}i_{sd} + \frac{R_r}{L_M}\Psi_r + w_sL_{ks}i_{sq}] \tag{2.65}$$

$$\frac{di_{sq}}{dt} = \frac{1}{L_{ks}}[V_{sq} - R_{ks}i_{sq} + w_m\Psi_r - w_sL_{ks}i_{sd}] \tag{2.66}$$

$$\frac{d\Psi_r}{dt} = R_r i_{sd} - \frac{R_r}{L_M}\Psi_r \tag{2.67}$$

$$0 = R_r i_{sq} - w_{sl}\Psi_r \tag{2.68}$$

$$\frac{dw_m}{dt} = \frac{n_p(T_e - T_r) - Bw_m}{J} \tag{2.69}$$

$$T_e = \frac{3}{2} n_p L_M i_{sd} i_{sq} \tag{2.70}$$

Looking at (2.67) and (2.70) it can be appreciated that the two components of the stator current act separately on the rotor flux and torque, because the flux depends only on the component i_{sd} while the i_{sq} component acts only on the torque.

The behavior of the induction machine controlled by field orientation is thus similar to that of a DC machine: in this analogy, the direct component of stator current assumes the role of the excitation current and the quadrature component of the armature current. Of course, while in DC machine the two currents flow in two distinct windings, in this case the i_{sd} and i_{sq} are the components along the axes d and q of a unique single-phase system of currents: the transition from one to the other system is obtained through the formula of the space phasor.

The decoupling, obtained between the effects of the two components of the stator current, can simplify the control of the mechanical variables of the drive. In fact, if the rotor flux is kept constant with the aim of properly exploiting the iron, the torque is directly proportional to the quadrature component of stator current i_{sq} whose reference value can be directly derived from the desired value of the torque. However, acting on i_{sd} varying the flux may also change the torque value, but given the presence of the high time constant with which i_{sd} influences the flux ($\frac{L_M}{R_r}$), which is higher than the time constant between stator current and stator voltage ($\frac{L_{ks}}{R_{ks}}$), this mode is not suitable for a rapid adjustment of the torque.

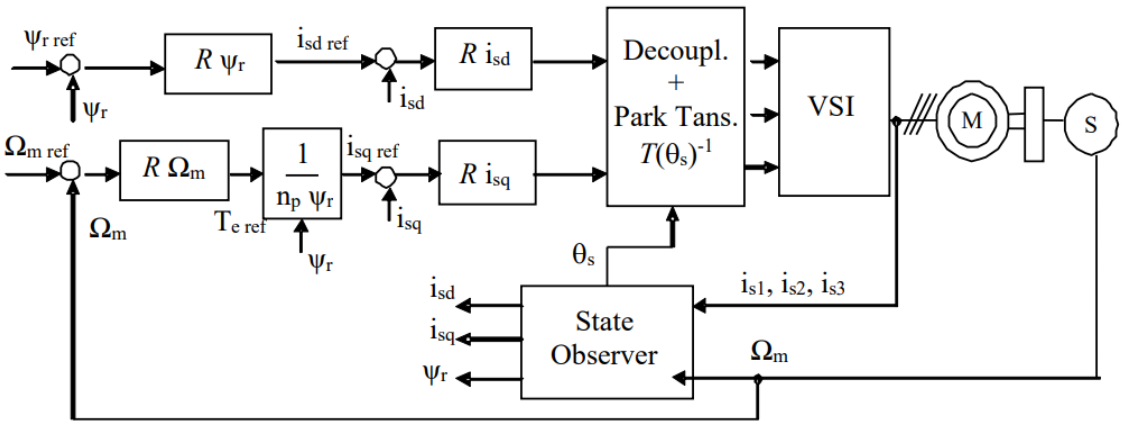

Figure 2.9: Diagram of FOC with Voltage Source Inverter

Figure 2.9 depicts the common structure of FOC when a Voltage Source Inverter (VSI) is used.

2.5 Electric Machine Controller Design

To properly track and control the speed and torque of the electric machine a controller is needed. The rotor speed is measured by a sensor and then is used in the control system. This is called a closed loop system, see Figure 2.10 . In a closed loop control system, a sensor measures the output of the process, and this measurement is compared to the desired reference. The difference between the measured output and the reference is called the error signal. The controller then uses this error signal to adjust the input to the process in order to bring the output closer to the reference.

By using the dq system, it is possible to decouple the control of the flux and torque in an IM, making it easier to design and implement control strategies. One of the benefits of using the dq system is that the controller type that are used are PI-controllers and I-controllers, the PI stands for Proportional and Integral, which is how the controller reduces the difference between requested value and measured value. The proportional part of the PI controller generates an output signal that is proportional to the error between the reference and the measured variable. The proportionality constant, known as the gain, determines how much the output changes in response to a given error. The proportional term provides an immediate response to changes in the error signal, helping to reduce the error quickly. On the other hand, the integral part helps to eliminate the steady-state error that is not corrected by the proportional part. The integral term is proportional to the integral of the error over time, which means that it accumulates the error over time and gradually increases the output until the error is reduced to zero.

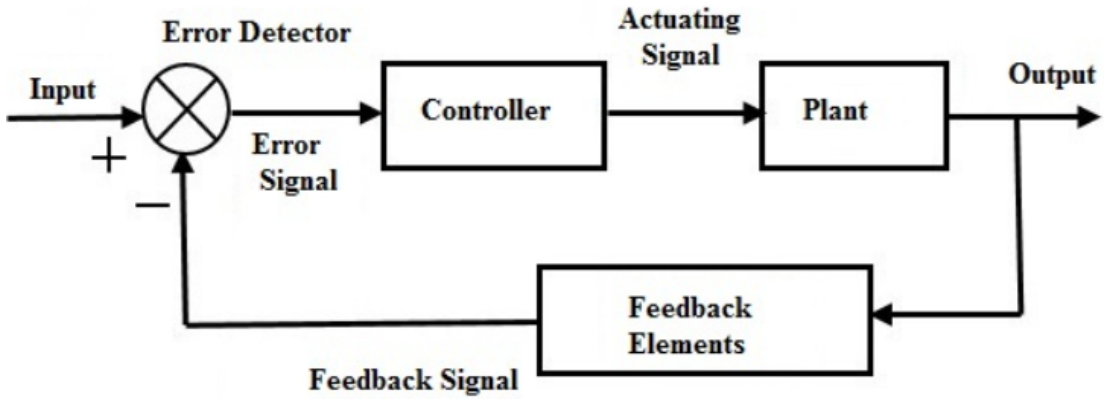

Figure 2.10: Closed loop control system scheme

In the IM R-FOC control technique, there may be up to 4 different controllers (flux, d-current, q-current and speed controllers). In the rotor resistance estimator case, a flux controller is needed due to that the step response from the current controller is too slow. The cascade design approach is very popular when it comes to designing the control of electrical machines [11]; this means that the bandwidth of the inner controller will at least be 10 times higher than the outer controller, for example, the q-current controller with respect to the speed controller.

For the selection of the bandwidth, it is crucial to know the system time constant and the rise time of the system. In the case of current controllers the time constant is very small, therefore, the bandwidth is quite high. Regarding the flux and speed controllers, the time constant are bigger, and thus the bandwidths are lower. Moreover, the phase margin in all the controllers is equal to 90 degrees, so the system is as stable as possible.

These controllers are typically designed as first-order low-pass filters to ensure that the step response does not have overshoot when attempting to reach the desired value. The speed at which a first-order system responds to a change depends on the system's bandwidth. The rise time, which represents the time taken for the system's output to transition from 10% to 90% of the requested value, is directly related to the system's bandwidth as

$$\tau_R = \frac{ln(9)}{\alpha} \tag{2.71}$$

The transfer function of the current controller is given by

$$tf_{curr} = \frac{1}{L_{ks}s + R_{ks}} \tag{2.72}$$

where L_{ks} is the stator leakage inductance and R_{ks} is the total resistance (rotor plus stator) in the four parameter inverse gamma model. The flux controller is designed with the following transfer function

$$tf_{flux} = \frac{R_r}{s + \frac{R_r}{L_M}} \tag{2.73}$$

where L_M is the mutual inductance and R_r is the rotor resistance in the four parameter inverse gamma model. Finally, the transfer function used for the speed controller is

$$tf_{speed} = \frac{1}{Js + \beta} \tag{2.74}$$

where J is the inertia and β is the friction coefficient.

2.6 MTPA

The MTPA tries to minimize the current needed to provide the maximum desired torque. Usually, in the IM, the stator copper losses due to Joule effect, are greater than iron and slip losses. Copper losses accounted for 40-65% of total losses, while iron and slip losses represent up to 25% and 15% respectively [8]. As a consequence of minimizing the copper losses, the electrical drive trains that use the MTPA as part of the control technique, will reach a higher efficiency, something that is important in the automotive industry.

The MTPA control algorithm may be divided into three different parts,

1. Current trajectory without reaching voltage limit.

   As long as the IM voltage is under the voltage limit the current trajectory will follow the MTPA line. In this project, the maximum voltage is defined as

   $$U_{smax} = \frac{U_{DC}}{\sqrt{3}} \tag{2.75}$$

   where U_{DC} is the dc link voltage. The maximum stator current I_{max} will define the current circle, which is a circle on the torque-speed plane that represents the maximum stator current that can be safely applied to the machine at any given operating point. The MTPA line for the inverse gamma model is derived from the stator current equation in polar form combined with the electromagnetic torque equation,

   $$T_e = \frac{3}{2} n_p L_M I_s^2 cos(\Theta) sin(\Theta) \tag{2.76}$$

   The maximum current angle Θ_{max} is obtained by doing the derivative of the torque equation with respect to the angle equal to zero.

   $$\frac{dT_e}{d\Theta} = 0, \tag{2.77}$$

   $$\Theta_{max} = 45^\circ \tag{2.78}$$

   The MTPA control algorithm should force the current angle to keep at 45 degrees until the voltage limit is reached.

2. Current trajectory when voltage limit is reached and flux weakening is applied.

   As the motor speed increases, the back electromotive force (back emf) of the machine will increase too since it is proportional to the speed (2.60). At a certain speed, called the base or rated speed, the back emf will be equal to that voltage limit U_{smax}. As a consequence, the IM is not able to go above the base speed by using more voltage. Thereby, the machine enters the flux weakening region, in which, by reducing the d-current the rotor flux decreases,

causing the back emf to be lowered. This allows the machine speed to increase.

Assuming that during steady state at high speed $w_m \approx w_s$, neglecting the voltage drop in R_{ks}, and neglecting $\frac{R_R}{L_M}\Psi_{rd}$ because $\frac{R_R}{L_M}$ is small, the stator voltage equations (2.59) and (2.60) can be simplified to

$$V_{sd} = -w_s L_{ks} i_{sq} \tag{2.79}$$

$$V_{sq} = w_s i_{sd}(L_{ks} + L_M) \tag{2.80}$$

The voltage limit can be calculated as

$$V_s = \sqrt{V_{sd} + V_{sq}} \tag{2.81}$$

Replacing (2.79) and (2.80) into equation (2.81) the voltage ellipse will be derived as

$$1 = \frac{i_{sq}^2}{(\frac{U_{s,max}}{w_s L_{ks}})^2} + \frac{i_{sd}^2}{(\frac{U_{s,max}}{w_s(L_{ks}+L_M)})^2} \tag{2.82}$$

which is an ellipse centered in the origin of the dq-plane with the semi-axes

$$r_q = \frac{U_{s,max}}{w_s L_{ks}} \tag{2.83}$$

$$r_d = \frac{U_{s,max}}{w_s(L_{ks} + L_M)} \tag{2.84}$$

It is clearly seen in (2.83) and (2.84) that the semi-axis of the ellipse are inversely proportional to the speed w_s. This means that the size of the voltage ellipse will decrease as the speed increases. To be within the voltage and current limits, the operating point must not exceed the current circle and the voltage ellipse. Figure 2.11 shows how the operating point of the IM changes as the speed increases.

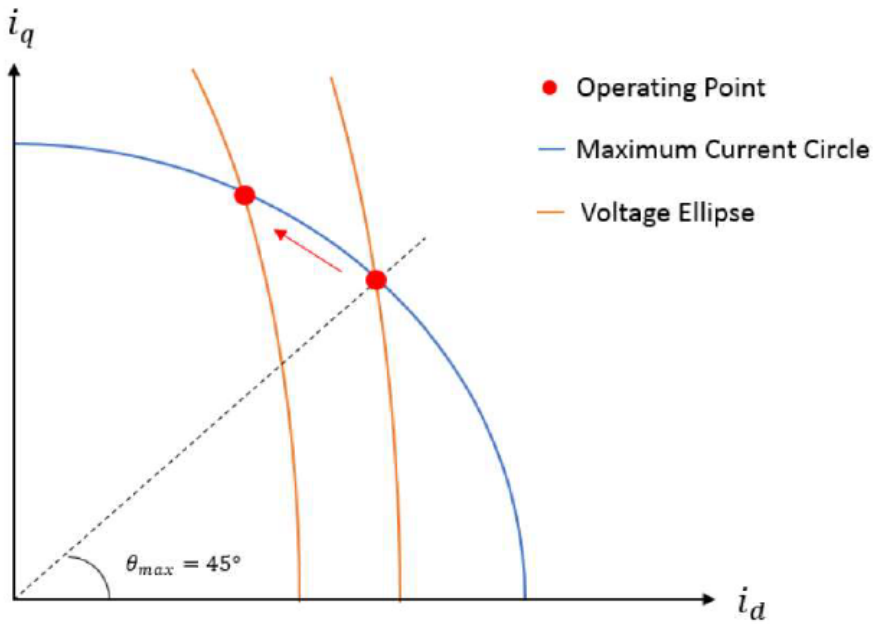

Figure 2.11: Operating points of the IM in region 2

Figure 2.11 shows how the IM operating point must leave the MTPA line at 45° to not exceed the voltage limit.

3. Current trajectory at speeds above the maximum slip frequency, that is the operating point in which maximum torque per voltage (MTPV) curve and current circle intersect. In this case, the current trajectory is minimized by following the maximum torque per voltage (MTPV) line and the voltage ellipses fall into the current circle as can be appreciated in Figure 2.12.

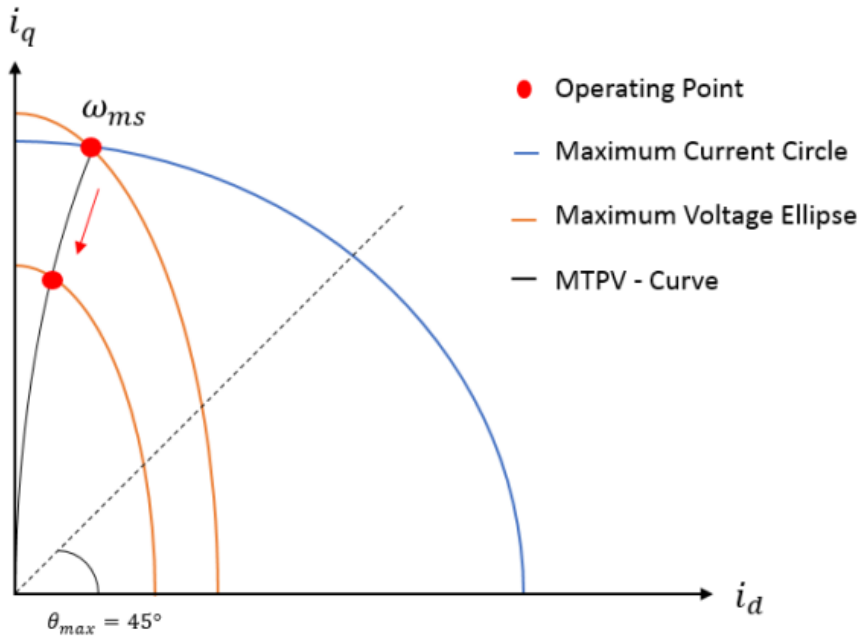

Figure 2.12: MTPV and operating points of the IM in region 3

The operating point enters the third region when the speed reaches the maximum slip frequency in region 2. Having higher slip for a certain voltage gives higher torque, but if the slip goes beyond the maximum allowable value the torque will go into the unstable control region. Assuming steady state and neglecting the voltage drop in the stator resistance, the torque in this region can be calculated by introducing the d and q currents, obtained from the d and q voltages equations, into the electromagnetic torque equation,

$$T_e = -\frac{3n_p L_M U_{smax}^2}{2w_1^2 L_\sigma (L_\sigma + L_M)} cos(\Theta_v) sin(\Theta_v) \tag{2.85}$$

The maximum voltage angle Θ_{vmax} is obtained by doing the derivative of the torque equation with respect to the angle equal to zero.

$$\frac{dT_e}{d\Theta_v} = 0, \tag{2.86}$$

$$\Theta_{v,max} = 135° \tag{2.87}$$

The MTPV control algorithm should force the current angle to keep at 135 degrees until the maximum speed is reached.

2.7 Model Reference Adaptive System

The MRAS is estimation technique which is based on calculating a quantity in two different ways. One of them depends on rotor resistance (adaptive model) and the other one is independent on it (reference model). Then, both quantities are subtracted to obtain the error, which will be fed into an adaptation mechanism, which usually is a PI controller. However, in this thesis, the adaptation mechanism will be an I-controller. The output of the adaptation mechanism is the estimated quantity, which at the same time will be an input of the adaptive model, closing the loop. Furthermore, the estimated quantity can vary; sometimes it directly represents the rotor resistance, while in other cases, such as this one, it corresponds to the variation of slip frequency. Finally, in this case, the Indirect Field Orientation (IFO) approach will be used in order to estimate the rotor resistance value. The basic structure of the MRAS is presented in Figure 2.13.

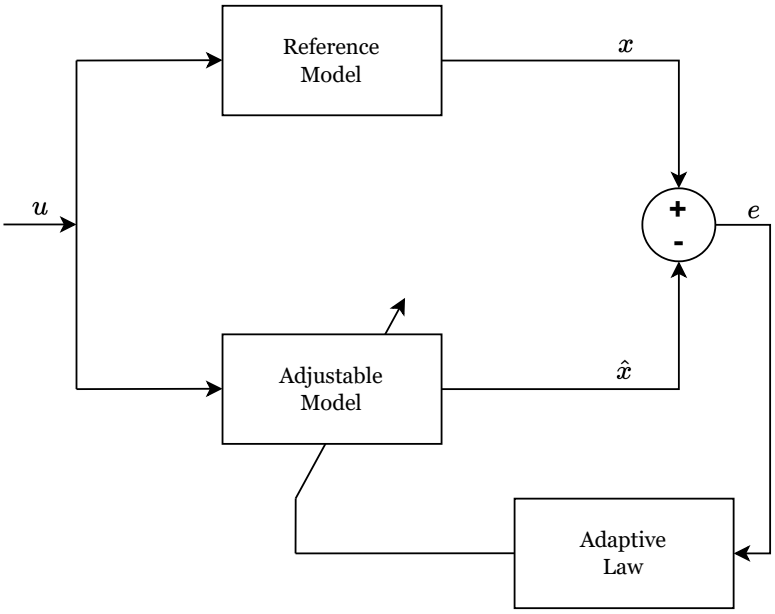

Figure 2.13: Basic structure of MRAS

The reactive instantaneous power, Q_{ref}, in the reference model is given by

$$Q_{ref} = V_{s\beta} i_{s\alpha} - V_{s\alpha} i_{s\beta} \tag{2.88}$$

The theoretical development of the proposed MRAS scheme is based on the IM inverse gamma model equations for the d and q reference frame. It is well known that the real and imaginary stator voltage in the dq reference frame for an IM are given by

$$V_{sd} = R_{ks} i_{sd} + L_{ks} \frac{di_{sd}}{dt} - \frac{R_r}{L_M} \Psi_r - L_{ks} w_s i_{sq} \tag{2.89}$$

$$V_{sq} = R_{ks} i_{sq} + L_{ks} \frac{di_{sq}}{dt} + w_m \Psi_r + L_{ks} w_s i_{sd} \tag{2.90}$$

where $w_s = w_m + w_{sl}$. Substituting (2.89) and (2.90) into (2.88), the estimated instantaneous reactive power (Q_{est}) which depends on rotor resistance and stator frequency is

$$Q_{est} = L_{ks}(\frac{di_{sq}}{dt}i_{sd} - \frac{di_{sd}}{dt}i_{sq}) + L_{ks}w_s(i_{sd}^2 + i_{sq}^2) + w_m\Psi_r i_{isd} + \frac{R_r}{L_M}\Psi_r i_{isq} \qquad (2.91)$$

Furthermore, the IFO condition $\Psi_{rd} = L_M i_{sd}$ and $\Psi_{rq} = 0$ can be substituted in (2.91) which gives

$$Q_{est} = L_{ks}(\frac{di_{sq}}{dt}i_{sd} - \frac{di_{sd}}{dt}i_{sq}) + L_{ks}w_s(i_{sd}^2 + i_{sq}^2) + w_m L_M i_{sd}^2 + R_r i_{sd} i_{isq} \qquad (2.92)$$

To simplify the adjustable model of the reactive power, steady state is assumed, therefore, the derivatives terms will be neglected from (2.92), obtaining as a result

$$Q_{est} = L_{ks}w_s(i_{sd}^2 + i_{sq}^2) + w_m L_M i_{sd}^2 + R_r i_{sd} i_{isq} \qquad (2.93)$$

The adaptation mechanism relies on the Hyper-stability concept [20], which mainly concerns the stability properties of a class of feedback systems as presented in Figure 2.14. The system is going to be considered as globally stable if the following two conditions are fulfilled.

1. The transfer function of the feedforward linear time invariant block must be strictly positive real.
2. The nonlinear time-varying block satisfies the Popov's integral inequality

$$\eta(0, t_1) = \int_0^{t_1} v^T w dt \geq -\gamma^2 \qquad \forall t_1 > 0 \qquad (2.94)$$

where v is the input vector, w is the output vector of the feedback block, and γ^2 is a finite positive constant.

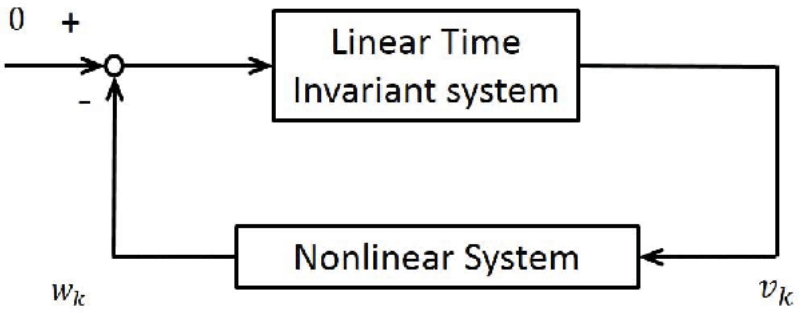

Figure 2.14: Nonlinear feedback system

2.8 High Frequency Signal Injection

The high frequency signal injection (HFSI) control is a technique for controlling the speed and torque in IM using high frequency signals that are injected in the stator windings. Due to the injected signals, a secondary magnetic field in the rotor that interacts with the fundamental magnetic field produced by the stator may be obtained. By controlling the amplitude and phase of the high frequency signals, it is possible to control the speed and torque of the machine, even at low speeds and high loads.

There are several different methods for implementing HFSI control, including current pulse injection, voltage injection and harmonic injection [3], [21], [22]. All of these methods are different in the way that the high frequency signals are injected into the stator windings, and each has its own advantages and disadvantages depending on the specific application. In this thesis, the high frequency current injection will be implemented with the aim of estimating the rotor resistance.

The direct axis stator current, i_{sd} is usually chosen because it does not impact the torque. As previously explained, the time constant with which i_{sd} influences the flux is quite high ($\frac{L_M}{R_R}$), therefore a change in i_{sd} will not affect the torque. The stator d-current is in phase with the stator voltage. Another reason for choosing i_{sd} for HFSI is that provides a strong coupling between stator and rotor. The high frequency signals create it's own magnetic field which induces a high frequency current in the rotor bars. This field will interact with the magnetic field that is created by the torque producing d-current. This high frequency current may be used to analyze and extract useful information from the IM, such as fault detection (rotor bars defects or winding faults) and parameter identification (stator resistance or magnetizing inductance) among others.

The injected signal usually has a square or sinusoidal waveform with a frequency that is different from the electrical frequency of the machine. The frequency is usually several kHz to several tens of kHz.

To inject the high-frequency signal, the inverter is controlled using pulse-width modulation (PWM) techniques to generate a high-frequency alternating current (AC) signal. The PWM signals are generated using a high-speed microcontroller or digital signal processor (DSP) that is programmed to produce the desired waveform.

The injected signal is typically superimposed on the existing stator current waveform, which consists of the fundamental frequency component and other harmonic components. The injected signal can be added to the stator current by controlling the amplitude and phase of the injected signal using the PWM signals.

This control technique has several advantages [3] over other methods of machine control. Some of the main advantages are:

1. Non-invasive: It is a non-invasive technique that does not require physical contact with the machine. This makes it easier to implement and maintain than other methods that require sensors.
2. Low cost: It can be implemented using existing hardware, such as a current source inverter (CSI), which makes it a relatively low-cost solution for machine control and monitoring.
3. Flexibility: This technique can be used in a wide range of applications, including speed and position estimation, fault detection and diagnosis, and control of IM. It can be applied to various machine sizes and types, including single-phase and three-phase machines.
4. Accuracy and reliability: High-frequency current injection provides accurate and reliable information about the machine's operation, including rotor speed, rotor resistance, and rotor bar defects. This information can be used to optimize machine performance and reduce the risk of failure.

These advantages make this control technique a valuable option for machine control and monitoring in different applications.

3

Case set-up

The machine that will be analyzed during this project is an IM. The AC machine models are obtained using prerequisite mathematics in relation to what is called the unified theory of electrical machines (based on Maxwell equations). The aim of this theory is that the control technique of a DC machine can be transferred to the AC machines.

First of all, in a simulation environment, an IM model is created. The software in which the simulations will be executed is MATLAB/SIMULINK. It is widely known that the Inverse Gamma model of an IM is the simplest representation of the IM, where the series inductance of the rotor side is cancelled using a proper transformation ratio. Afterwards, the PI controllers of the machine must be designed. Then, the MRAS and HFSI rotor resistance estimation methodologies will be implemented along with the IM model and the controllers. Finally, the rotor resistance estimation techniques will be compared between them.

The main parameters of the analyzed IM are presented in Table 3.1.

Table 3.1: Induction machine parameters

Parameters of the IM		
Designation	Parameter	Value
Stator resistance	R_s	2.8 mΩ
Rotor resistance	R_r	2 mΩ
Magnetizing inductance	L_m	0.85 mH
Stator leakage inductance	L_{sl}	0.05 mH
Rotor leakage inductance	L_{rl}	0.05 mH
Stator inductance	L_s	0.9 mH
Rotor inductance	L_r	0.9 mH
Inertia	J	0.051 kgm^2
Pole-pair number	n_p	2
Maximum stator current	I_s	900 A
Maximum speed	n_{max}	15400 RPM
DC voltage	U_{DC}	375 V

where stator and rotor inductance, L_s and L_r, are calculated as

$$L_s = L_{sl} + L_m \tag{3.1}$$

$$L_r = L_{rl} + L_m \tag{3.2}$$

As previously explained, in this project, the inverse gamma model of the IM will be used as the plant model. Due to the transformation ratio, k, the electric parameters of the IM will be modified for this model as shown in Table 3.2. Overall, the inverse gamma model is a simplified and computationally efficient model that can be used for real-time control applications.

Table 3.2: Induction machine inverse gamma model parameters

Inverse gamma model parameters		
Designation	Parameter	Value
Transformation ratio	k	0.944
Stator resistance	R_s	2.8 mΩ
Rotor resistance	R_R	1.8 mΩ
Total resistance	R_{ks}	4.6 mΩ
Magnetizing inductance	L_M	0.803 mH
Leakage inductance	L_σ	0.0972 mH

It is widely known in electric drives literature [1], that thermal effects can cause variations in the stator resistance, which may affect the machine's dynamic behaviour. Moreover, the magnetizing inductance, L_M, may vary due to the saturation of the core material. However, during this project, the stator resistance and magnetizing inductance will be kept constant and equal to its nominal value. The reason why the values are kept constant is that the stator resistance is normally known by measuring the stator winding temperature, and as a consequence there is no need of estimation, and in the case of the magnetizing inductance, the value will be kept equal to its nominal for simplicity. The MRAS needs to have an accurate value of V_d and V_q, which means that it is important to know the stator resistance but also the flux angle, which is related to the rotor resistance.

With regard to the rotor resistance, as it is the value to be estimated during this project, a linear increase variation will be applied as shown in Figure 3.1. This variation is intended to replicate the real rotor resistance variation caused by heating up. It is important to replicate the real behavior of the rotor resistance because it is a fundamental parameter in obtaining an accurate rotor flux angle, which is used to achieve the d and q voltages in the MRAS estimator. If the rotor resistance is incorrectly estimated, it can result in a loss of torque control. Moreover, the rotor resistance varies more than the stator resistance, and it is not easy to measure the rotor winding temperature. Hence, an accurate estimation of the rotor resistance value is crucial.

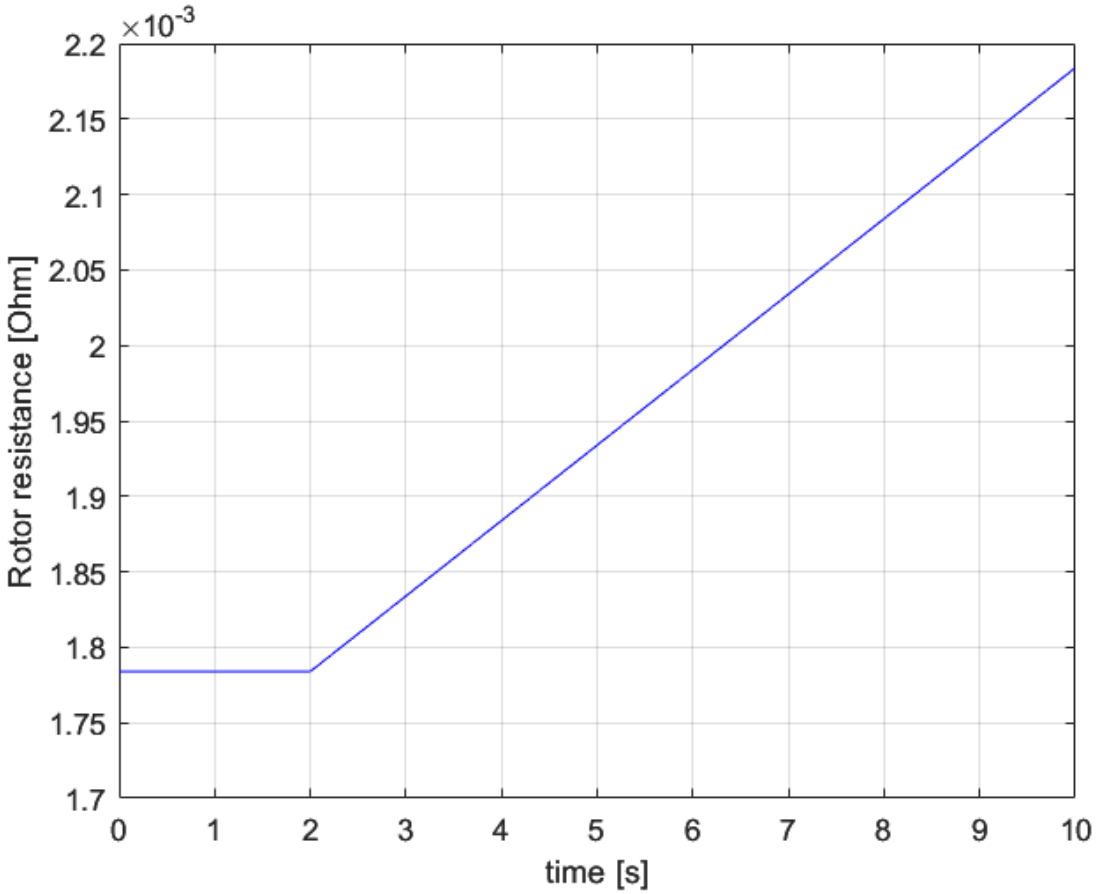

Figure 3.1: Rotor resistance variation

Figure 3.1 illustrates how the rotor resistance value changes with time due to a simulated thermal effect. In this case, the variation of the resistance is 0.05mΩ per second after the first two seconds, and during the first two seconds of simulation, the value is kept equal to the nominal value, R_R.

4

Analysis

4.1 Model Reference Adaptive System Estimator

4.1.1 MTPA Implementation

The validation of the MTPA algorithm is carried out by sweeping the speed and torque vectors, w_r and T_e. The MTPA algorithm is developed in a MATLAB script, where the ultimate goal is to minimize the d and q stator currents once the maximum torque for a given speed is known.

The MATLAB script may be divided into the following steps,

1. Obtain the rated speed of the IM.

   It is well known in the electrical machine's literature [11], that the rated mechanical speed is equal to

   $$w_{m,rated} = w_{s,rated} - w_{sl,rated} \tag{4.1}$$

   Thus, firstly, the rated electrical frequency must be obtained from the voltage equation. It is also well known, that at rated speed, the voltage equation (2.80) must be strictly equal to zero, thereby the rated electrical frequency can be obtained assuming steady state and that i_{sd} and i_{sq} are equal to the maximum possible d and q current respectively.

2. Calculate the maximum torque produced by the IM sweeping the speed from the rated to the maximum value.

   MATLAB's function fmincon was used as the tool for solving optimization problems. This predetermined function is firstly used to calculate the maximum torque for a given speed. Thereby, the equation that will be defined as the one to maximize is the torque equation (2.48). It is very important to highlight that fmincon obtains the minimum value of the given equation. As a consequence, a negative sign must be applied in order to maximize the desired output, torque in this case. Furthermore, some constraints must be applied so that the optimization problem can be solved. In this case, the constraints are inequalities given by the maximum voltage and current values

   $$\sqrt{i_{sd}^2 + i_{sq}^2} - I_{max}^2 \leq 0 \tag{4.2}$$

$$\sqrt{(R_{ks}i_{sd} - w_s L_\sigma i_{sq})^2 + (R_{ks}i_{sq} + w_s(L_\sigma + L_M)i_{sd})^2} - U_{smax}^2 \leq 0 \qquad (4.3)$$

3. Calculate the minimum currents that will provide the desired torque.

   Once the maximum torque is calculated in step 2, an evenly spaced torque vector is created, from zero to the maximum torque, with the aforementioned resolution. Afterwards, the torque vector must be swept so that the minimum currents can be achieved for all the possible torques. Once more, "fmincon" function is used to minimize the current equation, $i_{sd}^2 + i_{sq}^2$, according to the maximum given torque. The constraints are the same inequalities used in the previous step (4.2) and (4.3), however, an equality constraint that guarantees that the minimize currents satisfy the reference maximum torque (4.4) must be add in this step

$$-T_{e,ref} + \frac{3}{2} npL_M i_{sd} i_{sq} = 0 \qquad (4.4)$$

In the following figure, the results from the implemented MTPA control algorithm are presented.

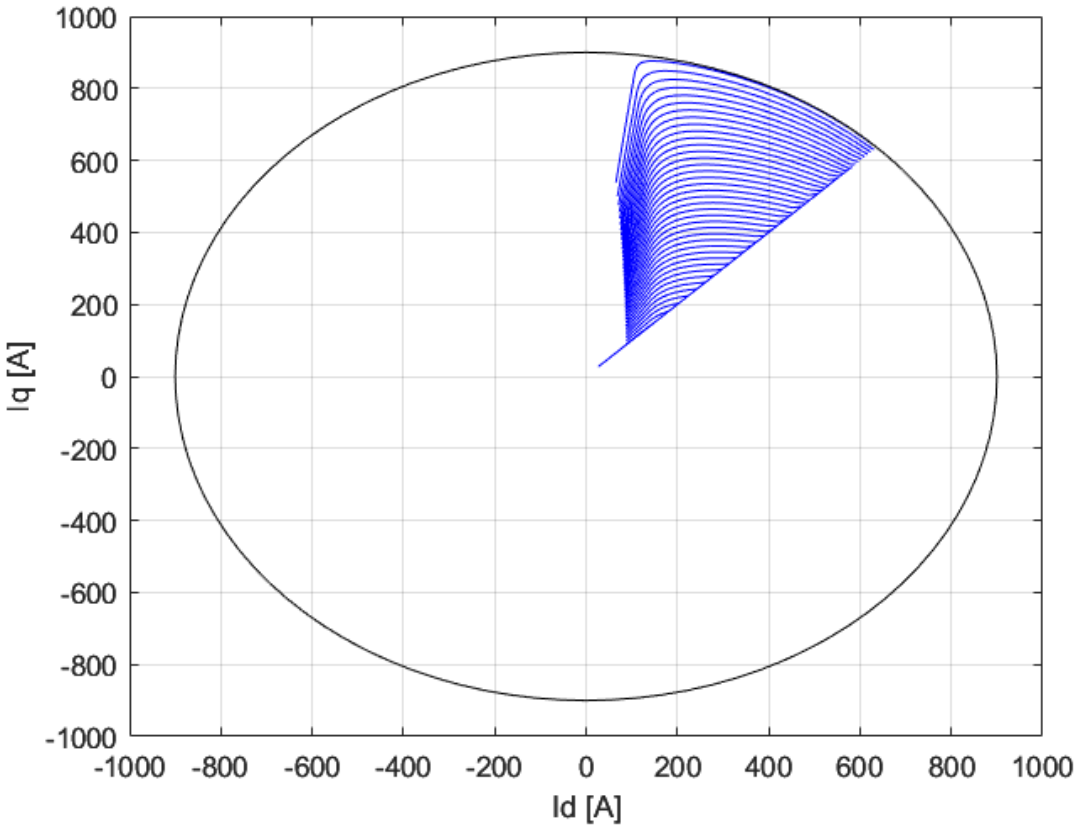

Figure 4.1: Currents trajectory during MTPA

Figure 4.1 depicts the three different regions of the current trajectory. The 45° line corresponds to region 1, the maximum current circle trajectory to region 2 and the 135° line to region 3. Therefore, although making some assumptions, it can be concluded that the MTPA control algorithm is working as expected in all the regions. In a vehicle application, the input to the motor controller is through the acceleration pedal which transforms into a torque input to the motor control algorithm. Hence, studying the trajectory of the currents with respect to torque is necessary.

The maximum possible torque, which will be use as a limit of speed's controller output, according to the implemented MTPA control algorithm is given by Figure 4.2.

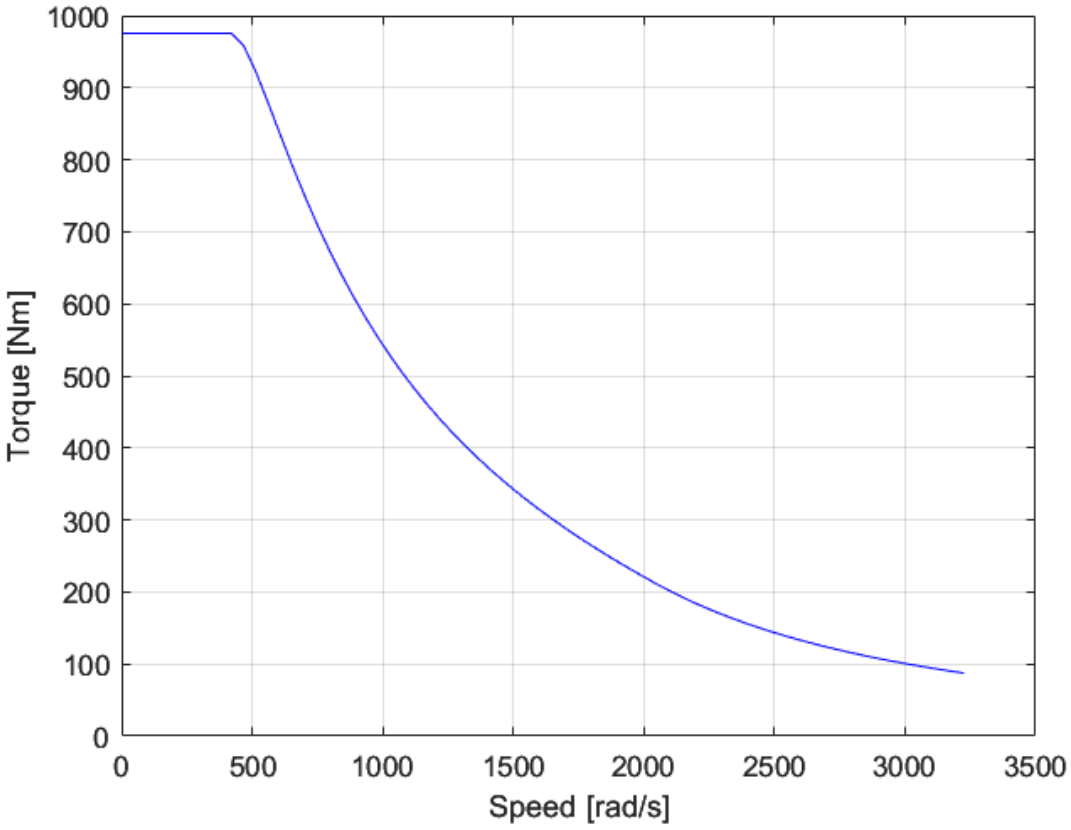

Figure 4.2: Maximum possible torque during MTPA

Figure 4.2 clearly illustrates the difference between the two main behaviours of the IM. Below the rated or base speed, the torque is maintained constant by exploiting the iron's magnetic properties to achieve a constant rotor flux as long as possible. Simultaneously, the stator q-current is held constant within the limit of the maximum allowable stator current. As a results, the electromagnetic torque will remain constant, since the flux and the q-stator current remain constant.

However, when the induction machine's speed beyond the base speed, it becomes necessary to decrease the d-stator current (2.67), and thereby, the rotor flux to obtain higher speeds without exceeding the voltage limit. This behaviour, which is referred to as flux weakening, is depicted in Figure 4.2. By reducing the rotor flux, the IM can achieve higher speeds while maintaining stable operation.

Figure 4.3 shows how the MTPA algorithm is implemented in Simulink. The goal of this algorithm, is to minimize the current required to provide the maximum desired torque, as previously explained. In this case, two different 2-D look-up tables are created, one for stator d and the other for stator q current. These currents will vary depending on the rotor speed and maximum reference torque for that speed. This results in a 2-D mesh for the stator d and q currents, as shown in Figures 4.4 and 4.5.

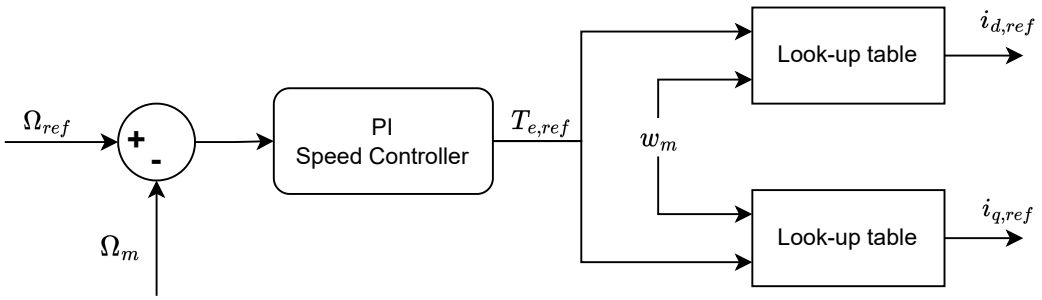

Figure 4.3: Implementation of the MTPA as a block diagram

In both Figures 4.5 and 4.6 the left horizontal axis stands for the electrical rotor speed in $[rad/s]$ and the right horizontal axis represents a dimensionless torque index, δ_T. To achieve it, first another index of the actual rotor speed is obtained. Afterwards, the index of the actual rotor speed will be the input of a maximum torque look-up table. In this way, the maximum possible torque is obtained. Finally, δ_T is obtained as the ratio between the reference torque (output of the PI speed controller) and the maximum possible torque. Figure 4.4 shows the process for obtaining the index δ_T.

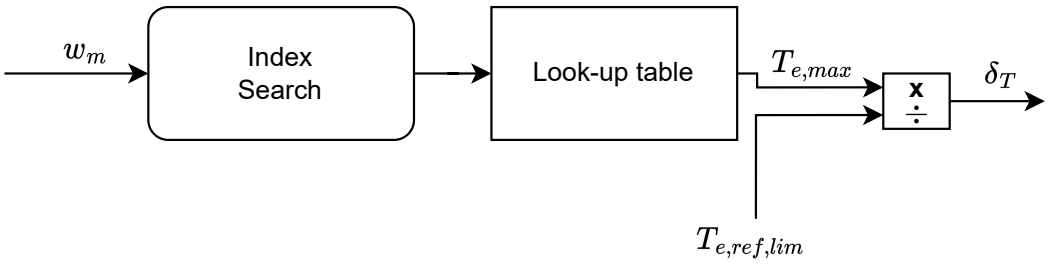

Figure 4.4: Index search structure

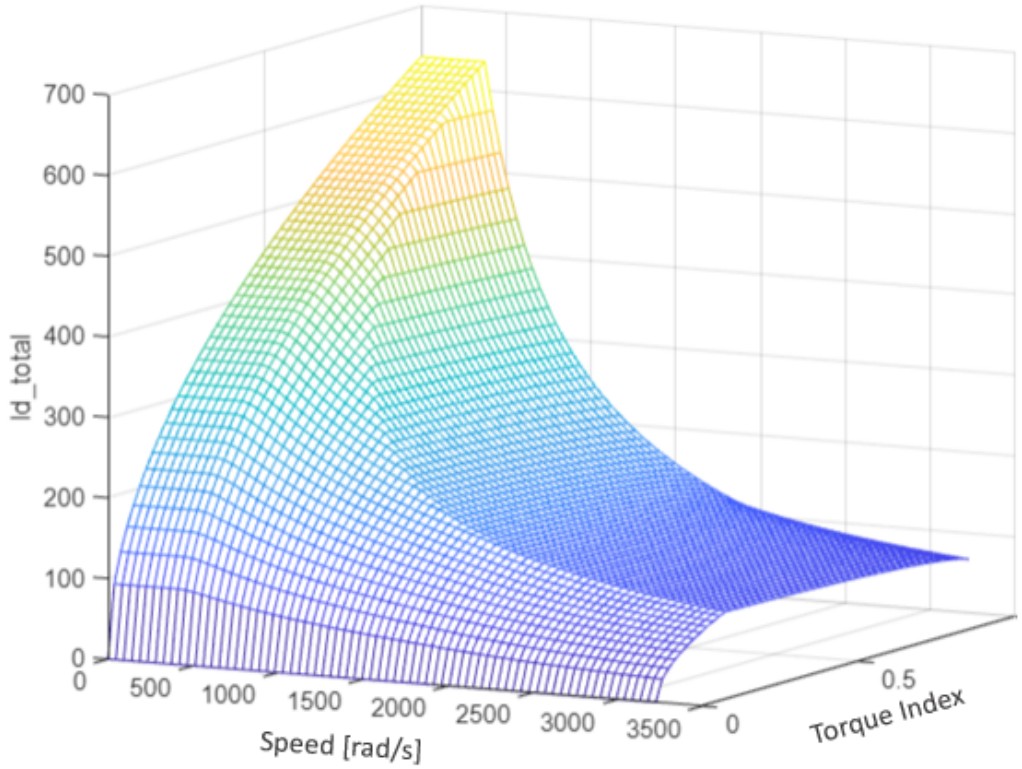

Figure 4.5: Stator d-current mesh

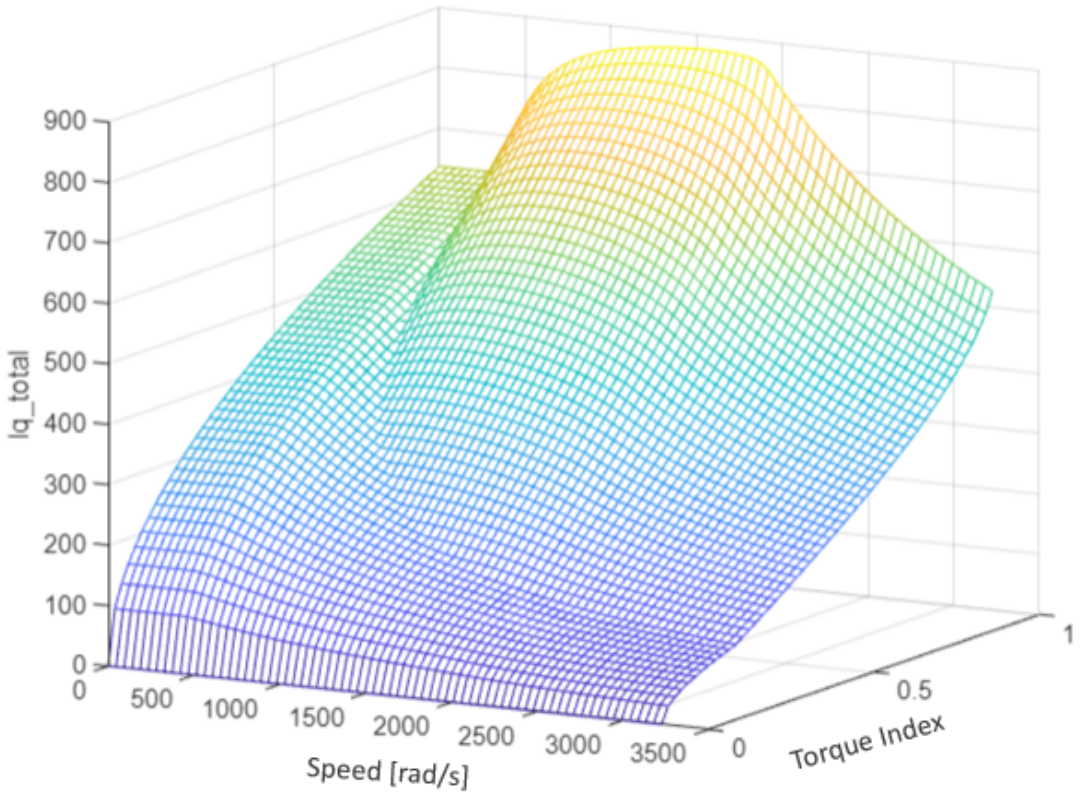

Figure 4.6: Stator q-current mesh

Figures 4.5 and 4.6 perfectly illustrates how for speeds lower than the rated speed, which in this case is around 400 rad/s, i_{sd} and i_{sq} are equal. For zero rotor speed and maximum torque these currents will be equal to $\frac{I_{s,max}}{\sqrt{2}}$.

When speed goes beyond the rated speed, it is clearly seen that the stator d-current reduces, and the machine enters in the flux weakening region. In order to guarantee that the commanded torque is reached, the stator q-current may increase as seen in Figure 4.6. Although i_{sd} reduces and i_{sq} increases, the total amount of stator current, I_s, is always within the limit established by the maximum current circle.

4.1.2 Model Reference Adaptive Control Algorithm

In the proposed MRAS, the reference and the adjustable models represent the instantaneous reactive power Q_{ref} and Q_{est}, respectively (see Figure 4.7). The reference model in this case is calculated as

$$Q_{ref} = V_{s\beta} i_{s\alpha} - V_{s\alpha} i_{s\beta} \tag{4.5}$$

where $i_{s\alpha}$, $i_{s\beta}$ are derived from the inverse Park transformation of dq stator currents used in IM model. However, both voltages, $V_{s\alpha}$ and $V_{s\beta}$, are obtained from the Clarke transformation of inverter's V_a, V_b and V_c.

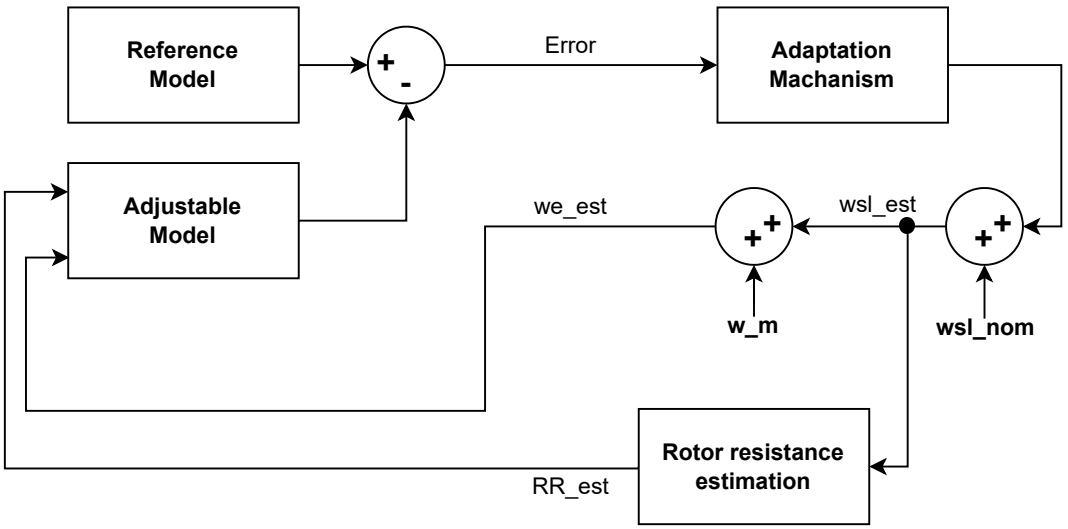

Figure 4.7: Modified MRAS scheme

The adjustable model of the reactive power will be given by the aforementioned equation, (2.90), in which the instantaneous reactive power is given by

$$Q_{est} = L_{ks} w_s (i_{sd}^2 + i_{sq}^2) + w_m L_M i_{sd}^2 + R_r i_{sd} i_{isq} \tag{4.6}$$

For stability analysis of the modified MRAS, Figure 2.13 is modified to Figure 4.8, in which,

$$w = -\rho_1 + (w_{sl,nom} + \delta w_{sl,est}(\varepsilon, t) + w_m)\rho_2 + w_m \rho_3 + \rho_4 \tag{4.7}$$

where,

$$\rho_1 = v_{sq} i_{sd} - v_{sd} i_{sq} \tag{4.8}$$

$$\rho_2 = L_{ks}(i_{sd}^2 + i_{sq}^2) \tag{4.9}$$

$$\rho_3 = \Psi_{rd} i_{sd} w_m \tag{4.10}$$

$$\rho_4 = \frac{R_{R,est}}{L_M} i_{sq} \Psi_{rd} \tag{4.11}$$

By introducing w in (2.91) and taking into account the general structure of the adaptation law, it can be affirmed that the inequality is satisfied. Thereby, a PI controller is enough to satisfy the second condition. In order to guarantee the first condition, the feedforward path gain must be real and positive. By manipulating the error sign the first condition is satisfied.

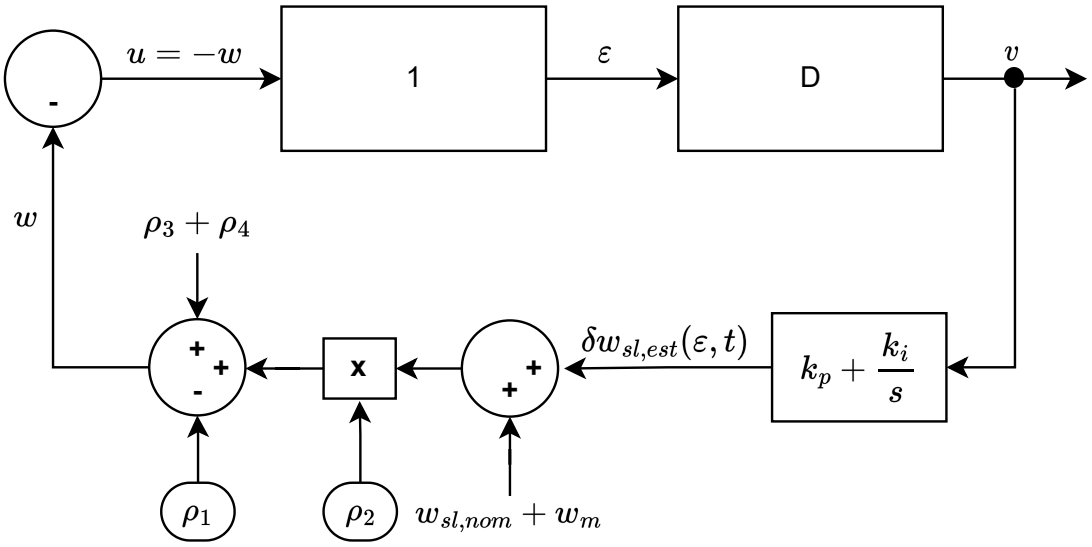

Figure 4.8: Equivalent feedback for modified scheme

The adaptation mechanism consists of an integral controller to avoid spikes in the variation of the slip frequency, which is related to the rotor resistance. The integral gain of the integral controller must be very small, otherwise the system will become unstable. It is well known in electric drives literature that rotor resistance pace of variation is very slow, due to the high time constant that relates the rotor flux and rotor resistance, and thus, the integral gain must be selected taking into account this fact. If a PI controller is selected to track the error signal, to avoid instability, the error must be first low-pass filtered.

Besides, to complete the adaptation mechanism, the nominal value of the slip frequency is determined (2.68), see Figure 4.9, to which the variation of the slip frequency will be added to obtain the estimated slip frequency, which is used to calculate the estimated value of the rotor resistance (input in the adjustable model) as shown in Figure 4.10. Then, the mechanical speed is summed to the slip frequency to achieve the electrical speed which is an input in the adjustable model, and thus, the loop is closed. Regarding the integral controller, maintaining the cascade design and assuming that the variations in the rotor resistance due to temperature variations are quite slow, the integral time constant will be much lower than the one calculated for the speed controller.

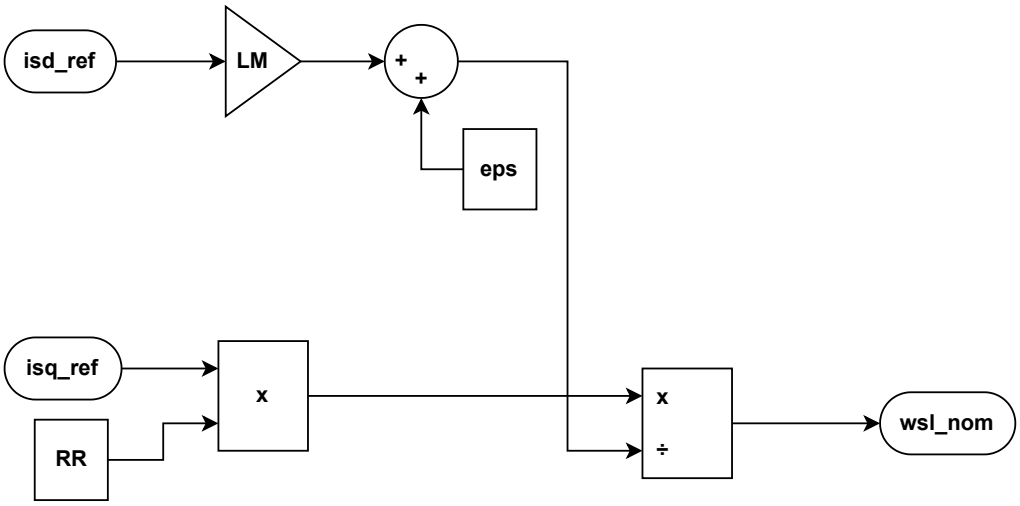

Figure 4.9: slip frequency calculation

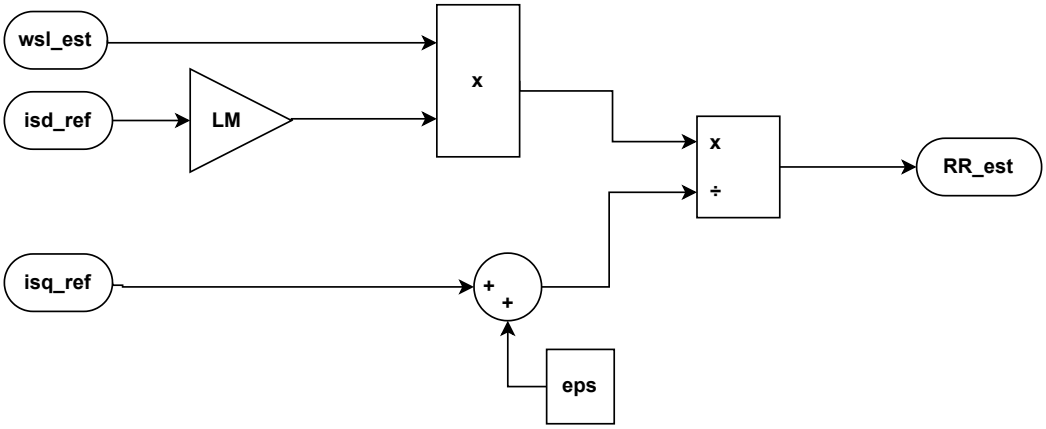

Figure 4.10: Rotor resistance estimator

The estimated slip frequency is used to calculate the rotor resistance value, which is needed to get the flux estimation (2.67), as shown in Figure 4.11. Finally, once the rotor resistance and rotor flux are estimated, the slip frequency is calculated, to which the mechanical speed is added to obtain the estimated electrical speed, which is integrated to achieve the estimated transformation angle.

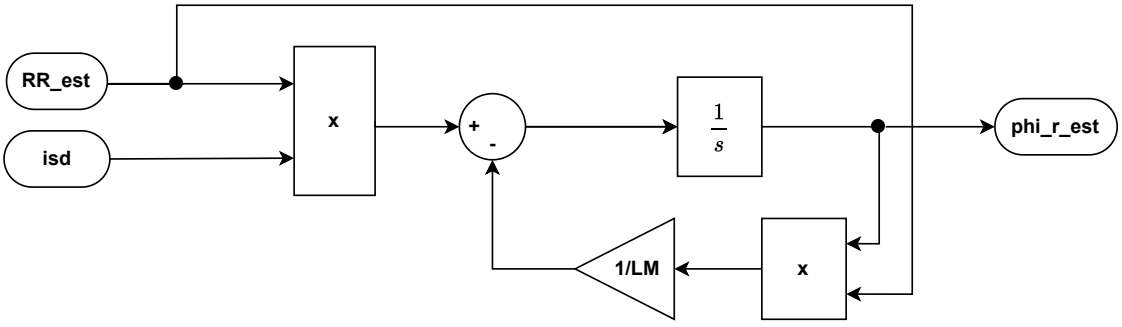

Figure 4.11: Rotor flux estimator

4.2 High Frequency Signal Injection

Regarding the high frequency signal injection (HFSI) method, in this project, rectangular pulses are added to the flux command reference current, i_{sd}. As a consequence the stator d-current will change rapidly without the rotor flux changing significantly, see Figure 4.12 and 4.13. Moreover, the change in rotor flux controlling current will affect the torque control current. As a result of the minor variations in the rotor flux and stator q-current, the real torque of the machine will have a slight variation due to the pulses, see Figure 4.16. Finally, due to the small variations that the real torque will have, the rotor speed will also experiment negligible variations due to the pulses, which will affect the output of the speed controller, $T_{e,ref}$. This signal will be used to estimate the rotor resistance value.

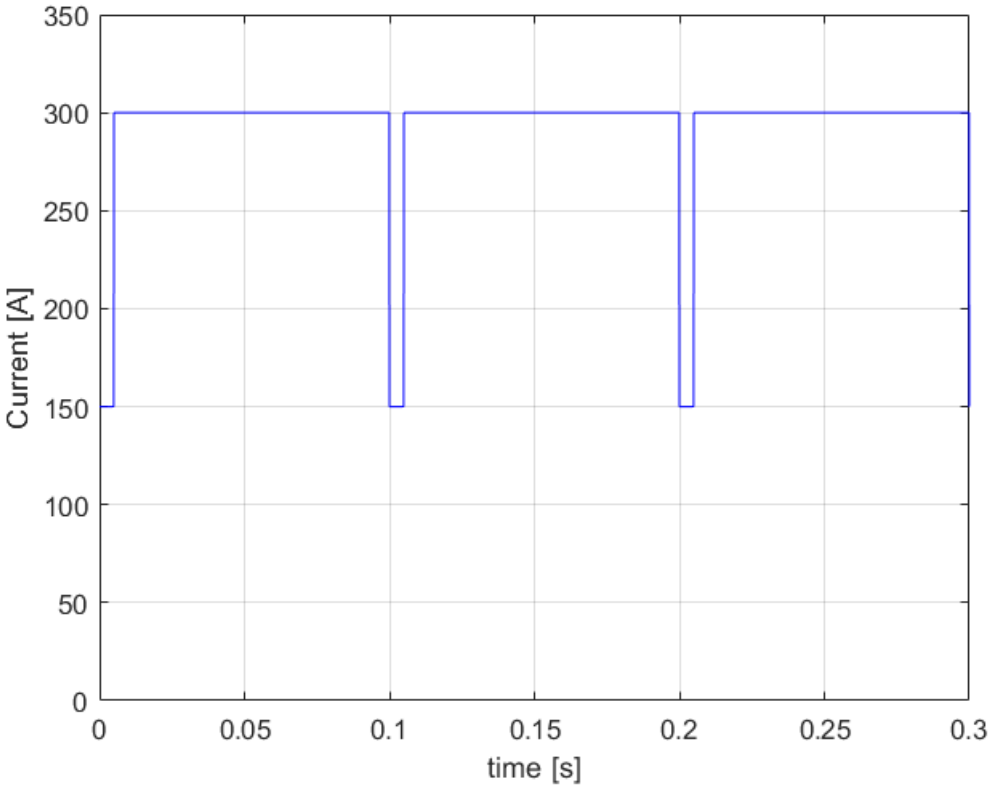

Figure 4.12: Stator d-current with high frequency pulses

Figure 4.12 depicts the stator d-current, which is equal to 300A and has negative pulses with a magnitude of 150A. The period of the pulses is 0.1s and the width is equal to 5% of the period. The added pulses in i_{sd}, will also affect i_{sq} due to the cross-coupling term. Figure 4.13 shows how the stator q-current increases when speed step is applied, and then reaches steady state. The operating point with this i_{sd} current is in the constant torque region of the torque-speed curve.

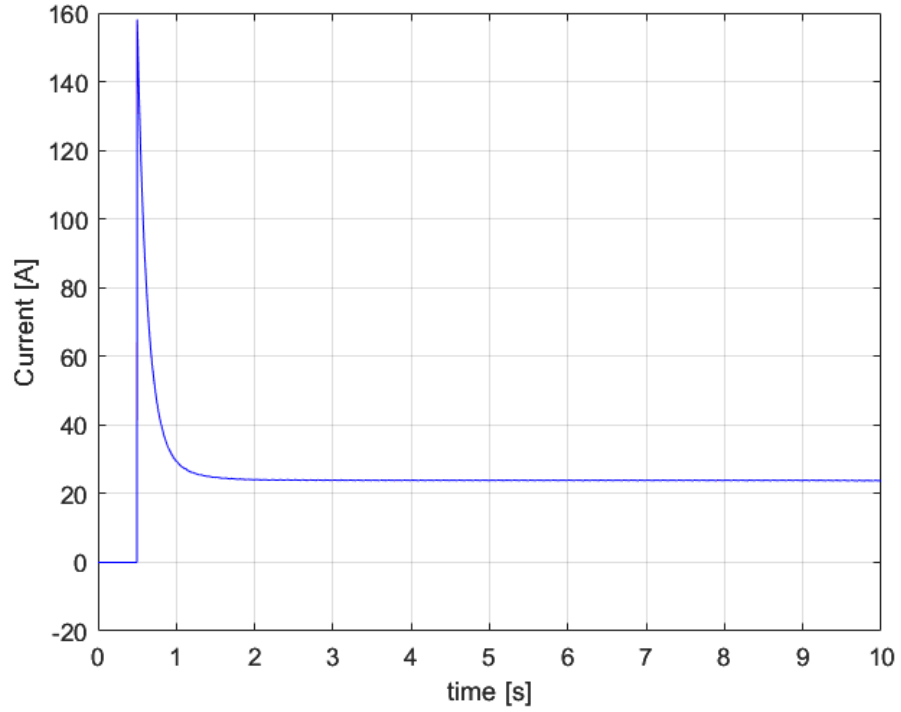

Figure 4.13: Stator q-current in HFSI

At first sight, it may appear, that the stator q-current is not affected by the pulses added in i_{sd}, however, zooming the steady state region, small variations emerge in i_{sq} as shown in Figure 4.14.

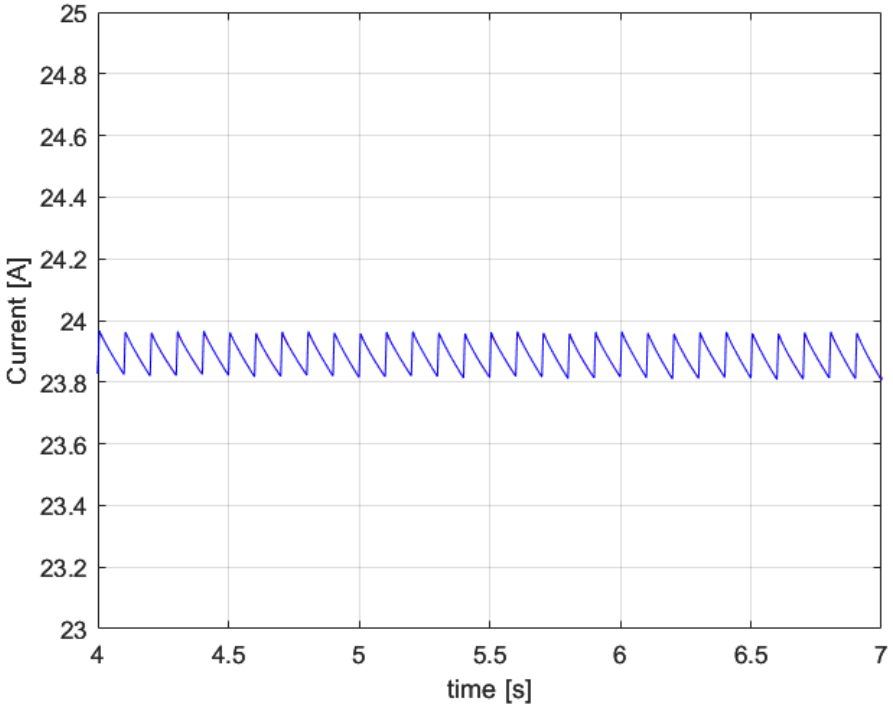

Figure 4.14: Stator q-current under HFSI during steady state

In this estimation technique, the rotor resistance estimated value will be obtained analyzing the reference demanded torque, which is the output of the speed PI controller. The following steps have been implemented to estimate the rotor resistance:

1. Sample the reference torque command at three points.
   a Start of the flux pulse
   b End of flux pulse
   c 50 samples after the flux pulse.
2. If sample (b) is greater than (a) and (c), then
$$\hat{R}_r(k+1) = \hat{R}_r(k) - \Delta\hat{R}_r$$
3. If sample (b) is less than (a) and (c), then
$$\hat{R}_r(k+1) = \hat{R}_r(k) + \Delta\hat{R}_r$$
4. Limit $\hat{R}_r(k+1)$ within half the value to twice the value of the nominal R_r.
5. Repeat from step 1 at the start of the next flux command pulse.

The $\Delta\hat{R}_r$ parameter is arbitrarily chosen, depending on the nominal value of the rotor resistance. In this project, $\Delta\hat{R}_r = 10^{-5}$.

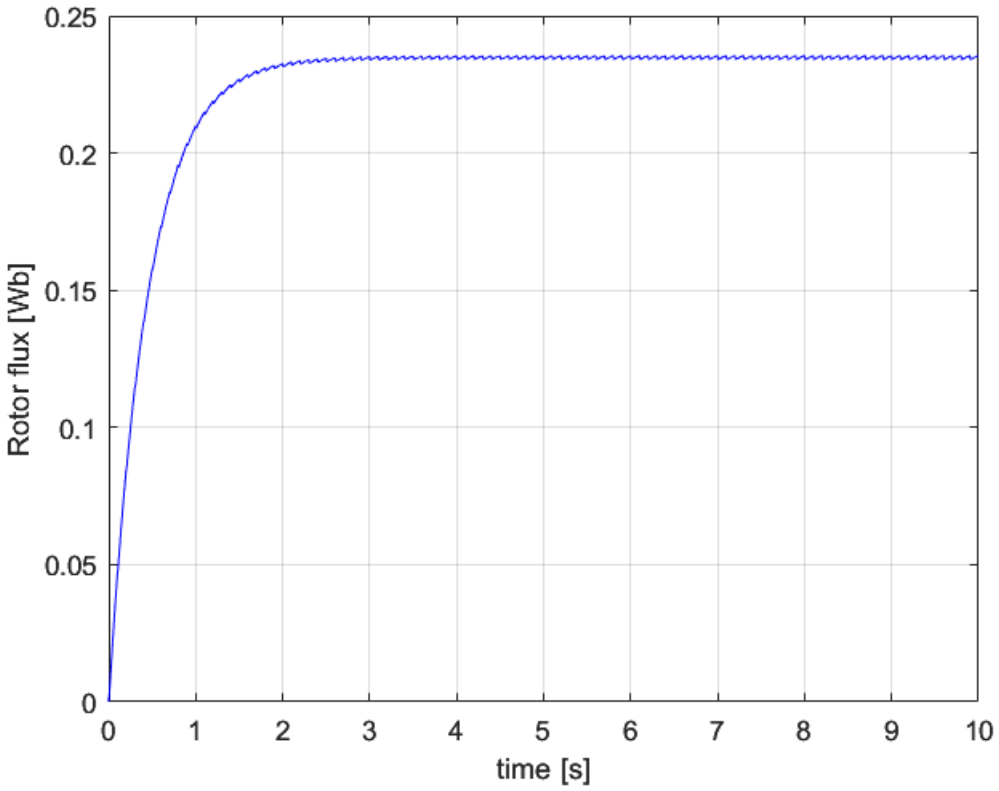

Figure 4.15: Rotor flux under HFSI

Zooming in Figure 4.15, the slight variation on the rotor flux due to the pulses added in the stator d-current can be appreciated in Figure 4.16.

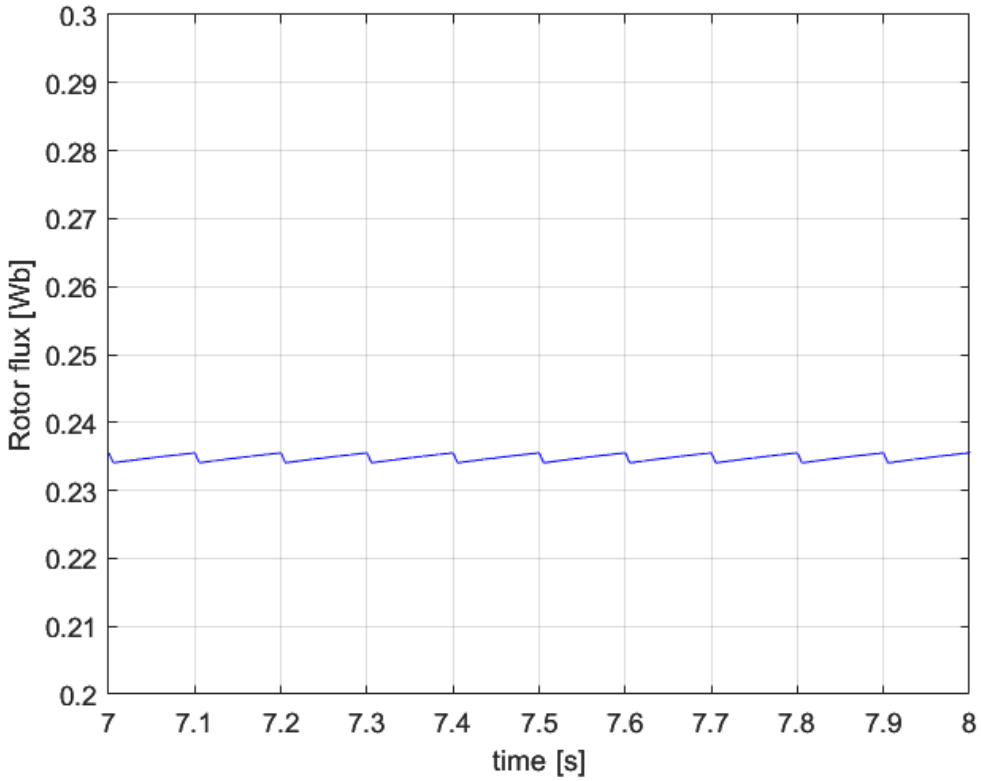

Figure 4.16: Rotor flux variation under HFSI during steady state

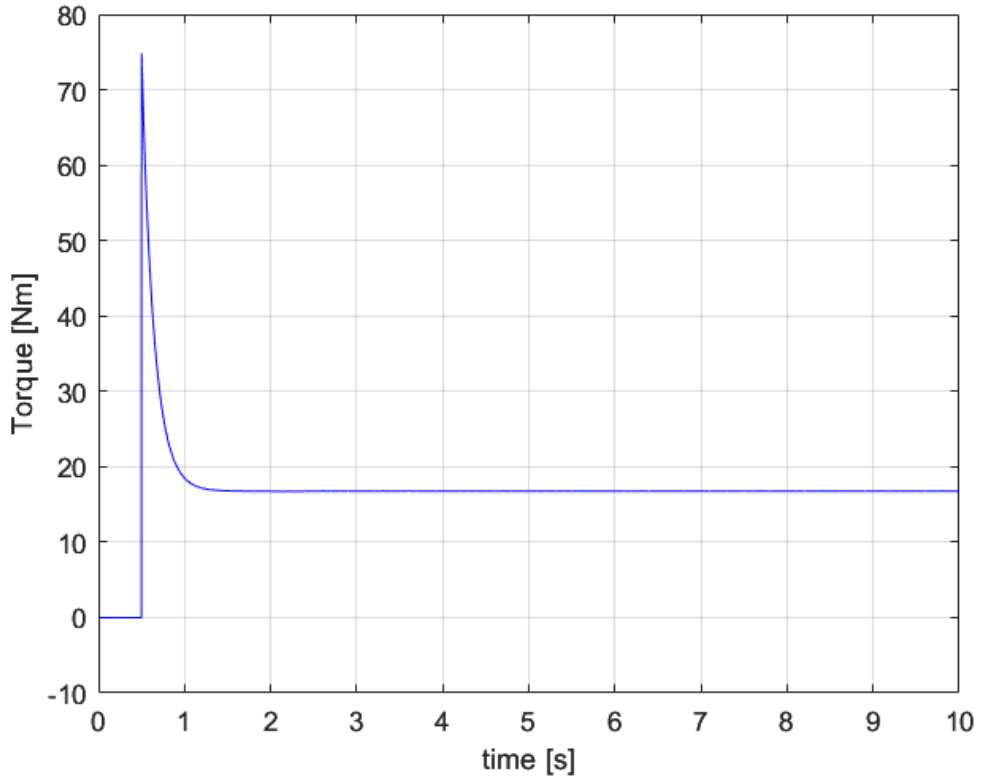

Figure 4.17: Electromagnetic torque variation under HFSI

Figure 4.17 illustrates the electromagnetic torque variation under HFSI, at first glance, it looks like it is perfectly constant, and thereby, not affected by the stator d-current pulses. However, by zooming in the steady state values of the electromagnetic torque, the slight variations due to the pulses added can be appreciated as shown in Figure 4.18.

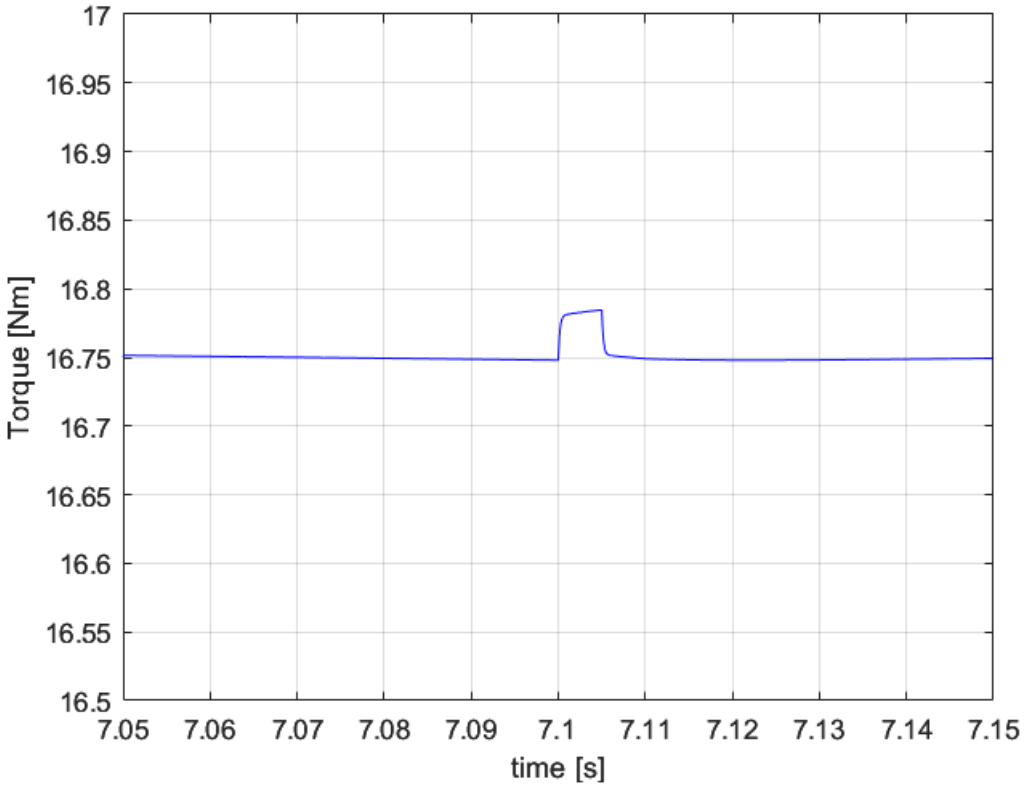

Figure 4.18: Electromagnetic torque variation under HFSI during steady state

Figure 4.18 shows how the added pulses in the stator d-current affect the electromagnetic torque of the IM. However, it can be clearly seen that the effect of the pulses is almost negligible on the torque, having a variation lower than 0.05Nm with each pulse.

5

Conclusions

5.1 Results from present work

This project was carried out with the goal of comparing different rotor resistance estimator techniques. To do so, two different rotor resistance estimators were analyzed in MATLAB/SIMULINK. The results of the analyzed rotor resistance estimators confirm that the analyzed estimators work properly and achieve a very close value to the varying rotor resistance value.

Firstly, the MRAS estimator is analyzed. The input to the MRAS is a mechanical speed step at 0.5 seconds as shown in Figure 5.1.

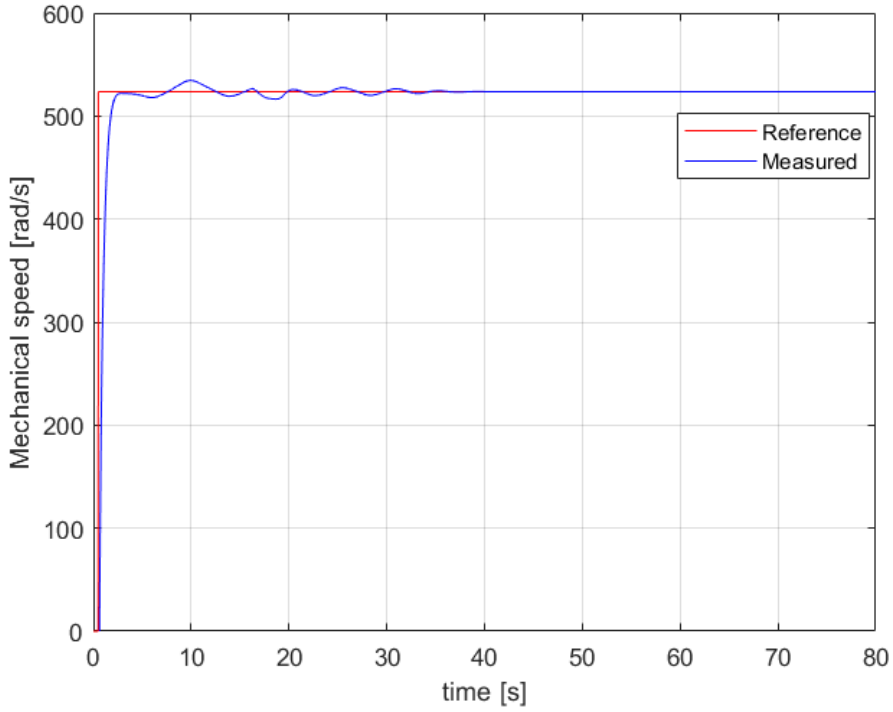

Figure 5.1: Speed step response in MRAS

Figure 5.1 shows the reference and measured mechanical speeds in $[rad/s]$. It can be clearly seen that although the system is a bit unstable in the beginning, it reaches steady state.

The instantaneous reactive power obtained from the reference and adaptive models described by (2.88) and (2.93) respectively, is shown in Figure 5.2.

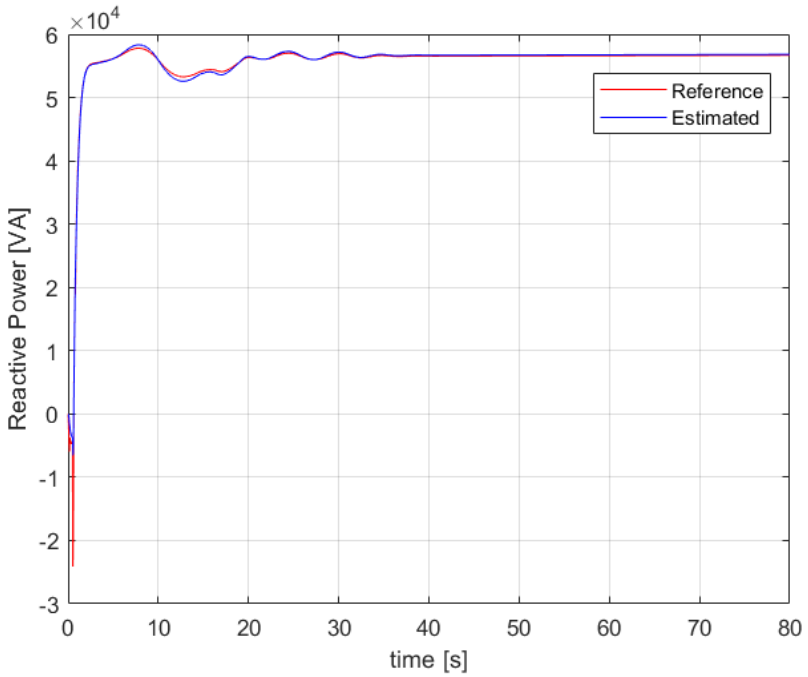

Figure 5.2: Reactive power from reference and adaptive models

After subtracting the reference and estimated instantaneous reactive power, the error is obtained. This error is then fed into an I-controller, and the resulting output is added to the nominal slip frequency to achieve the estimated slip frequency.

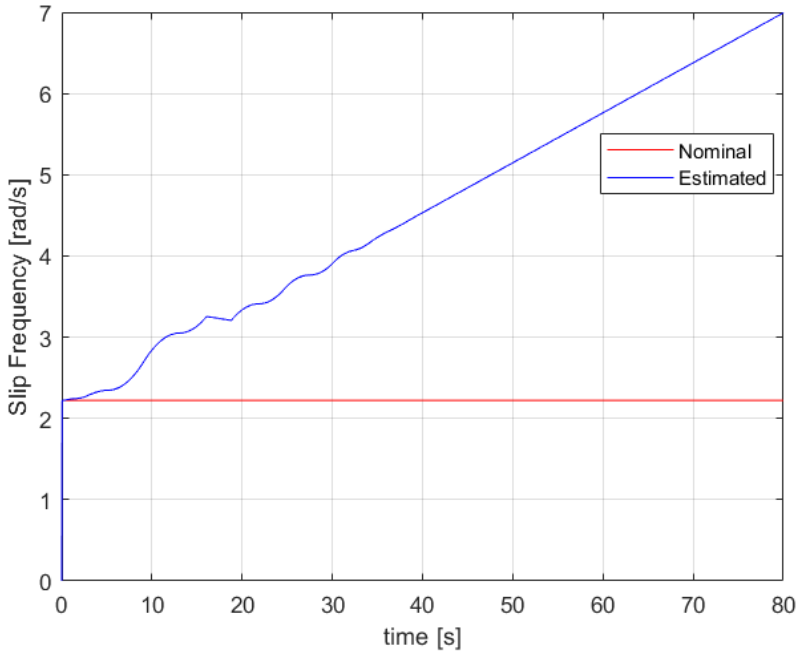

Figure 5.3: Nominal and estimated slip frequency for MRAS

Figure 5.3 depicts the nominal and estimated slip frequency. The nominal slip frequency corresponds to the nominal value of the rotor resistance, denoted as R_R. On the other hand, the estimated slip frequency is determined based on the estimated rotor resistance, which increases due to thermal effects on the rotor. As the rotor resistance progressively rises, the estimated value follows suit, leading to a linear increase in the estimated slip frequency.

Figure 5.4 depicts that after 2 seconds, the nominal value of the rotor resistance increases with a ramp, simulating the variation caused by thermal effects in the rotor resistance. It can be observed, that the estimated value closely follows the nominal value when the system reaches stability. The slight difference between the nominal and estimated values is due to PI controllers. By utilizing PID controllers, the error when applying a ramp could be reduced to zero.

However, if the rotor resistance reaches a steady-state value after rising from its nominal value, the PI controllers will ensure a zero steady-state error as shown in Figure 5.5. Furthermore, it can be seen, that when the rotor resistance matches its nominal value, the estimated value accuracy is remarkably high.

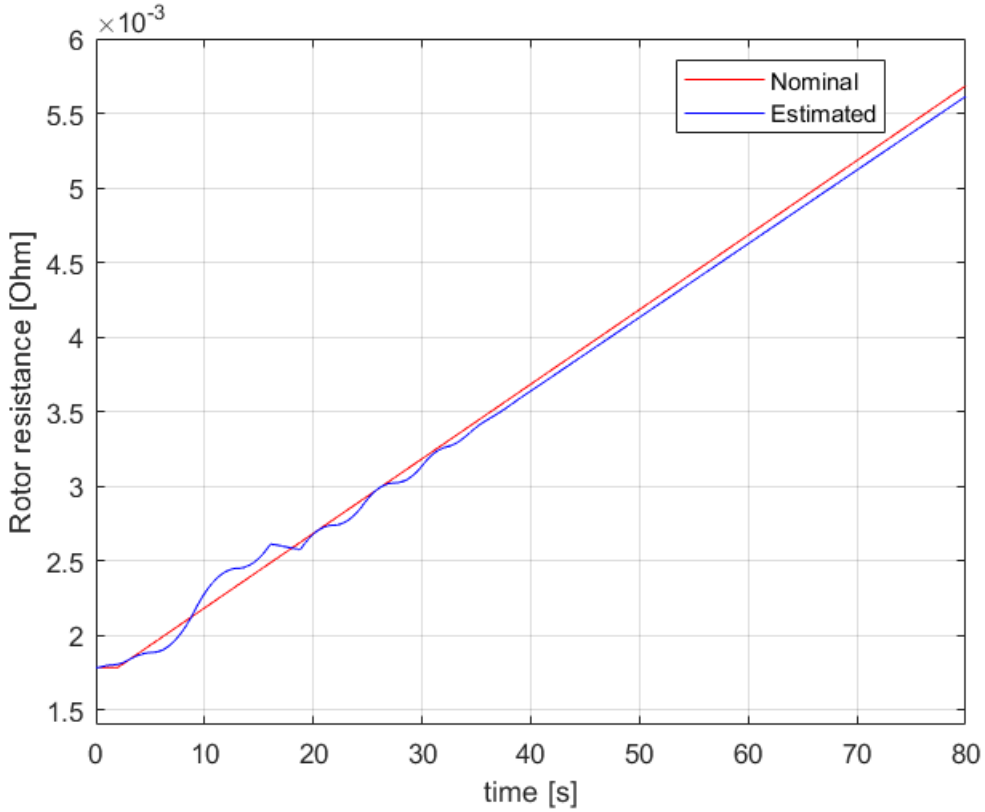

Figure 5.4: Rotor resistance estimation in MRAS

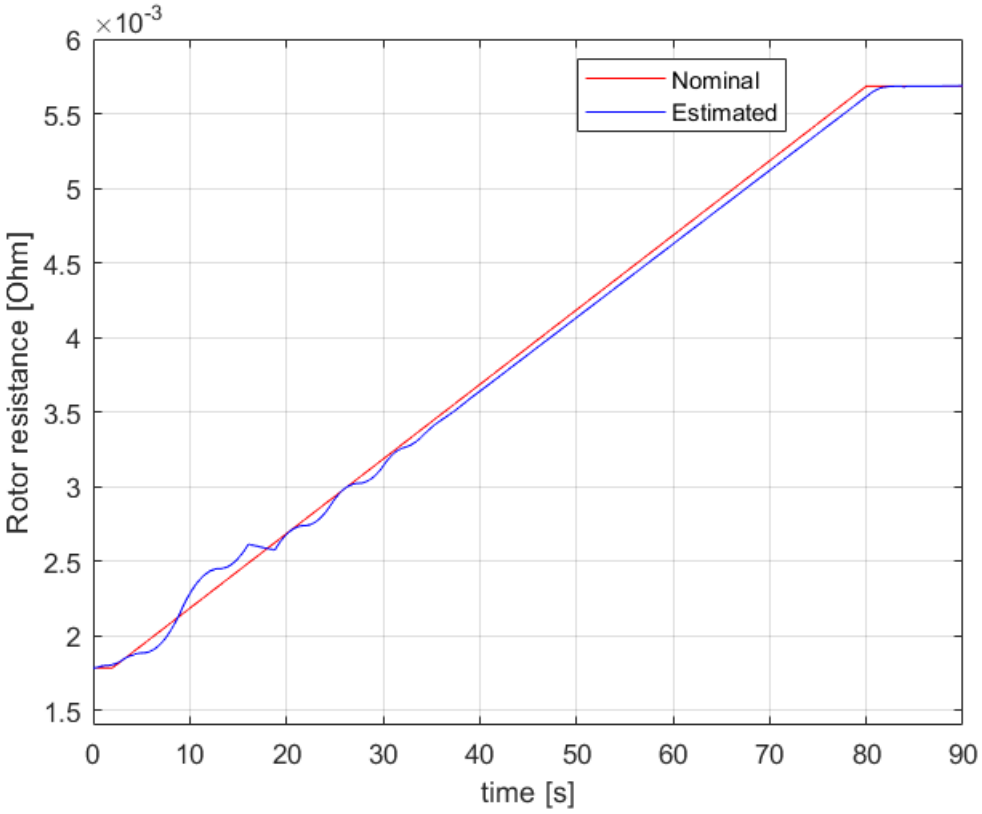

Figure 5.5: Rotor resistance estimation when steady-state is reached

The robustness that the reactive power MRAS presents against stator resistance variations, makes the different against other estimators in the case that a stator resistance estimator is not implemented. Regarding the MRAS, there is no need of implementing a stator resistance estimator, because the model itself eliminates the dependence on this parameter (4.6).

Secondly, the HFSI estimator is analyzed. The inputs to the HFSI estimator are; a mechanical speed step at 0.5 seconds as shown in Figure 5.6, and the i_{sd} current with the added pulses as shown in Figure 4.12.

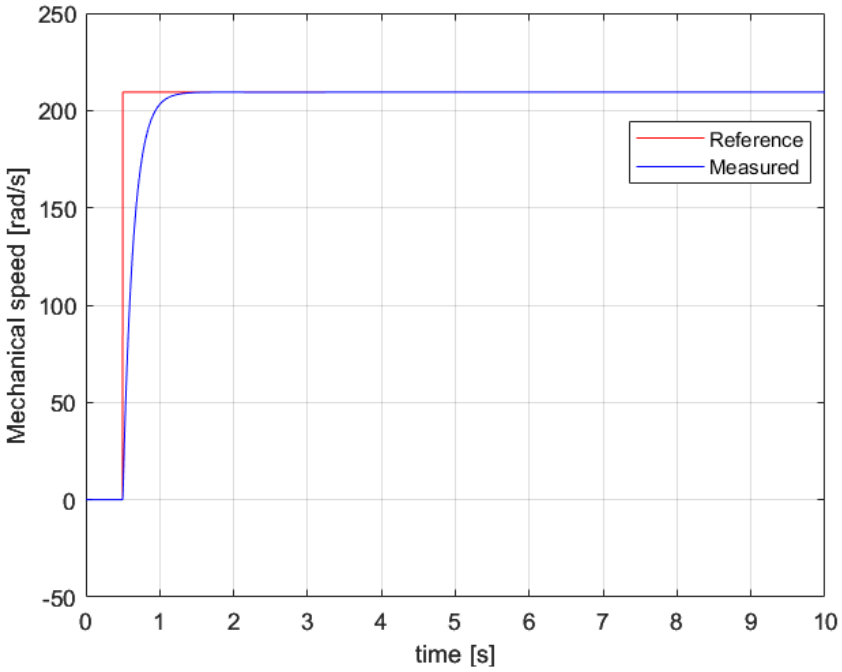

Figure 5.6: Speed step response in HFSI

Figure 5.6 illustrates the reference and measured mechanical speeds. It can be seen that the speed response corresponds with a first order system response. As previously explained, the reference torque command is sampled at three different points, see Figure 5.7. Depending on whether the second sampled torque is higher or lower than the other two, the rotor resistance will be increased or decreased by ΔR_R.

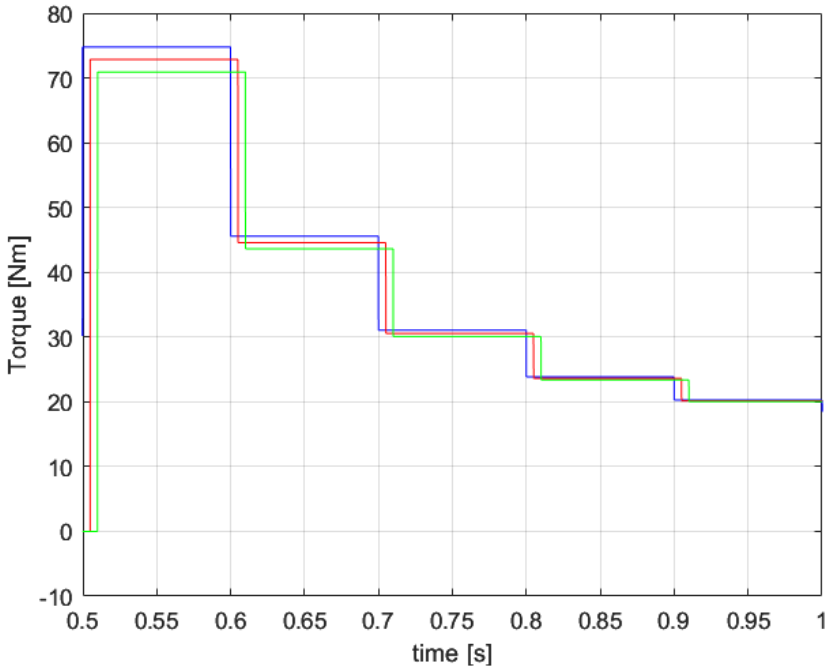

Figure 5.7: Sampled reference torque command at three different points

Bearing in mind the aforementioned rotor resistance estimation algorithm, Figure 5.8 and 5.9 illustrate how the rotor resistance is estimated during the HFSI estimator.

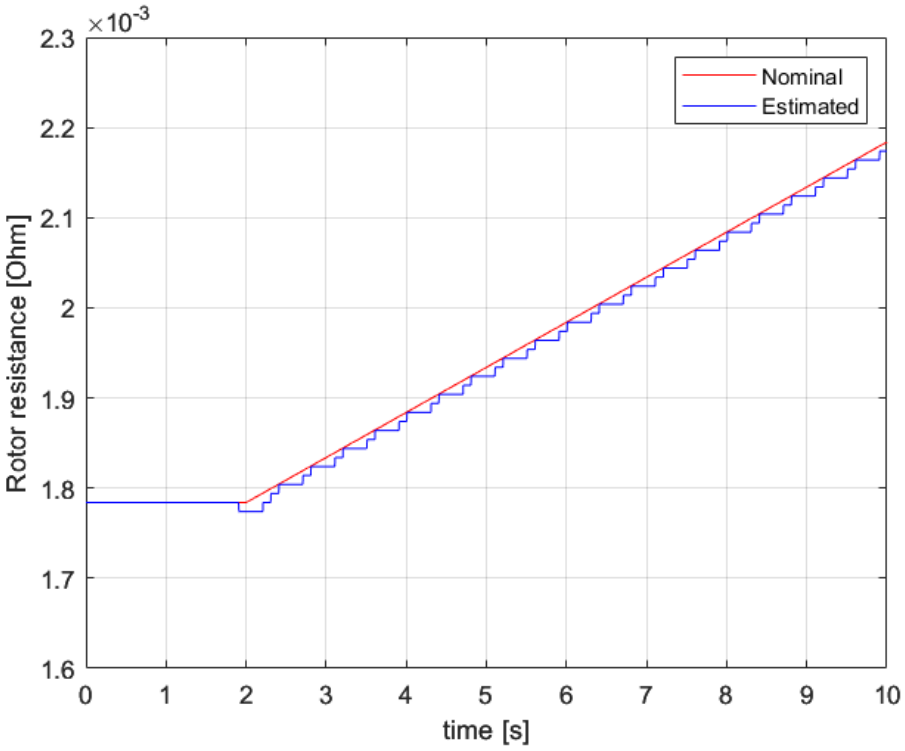

Figure 5.8: Rotor resistance estimation in HFSI

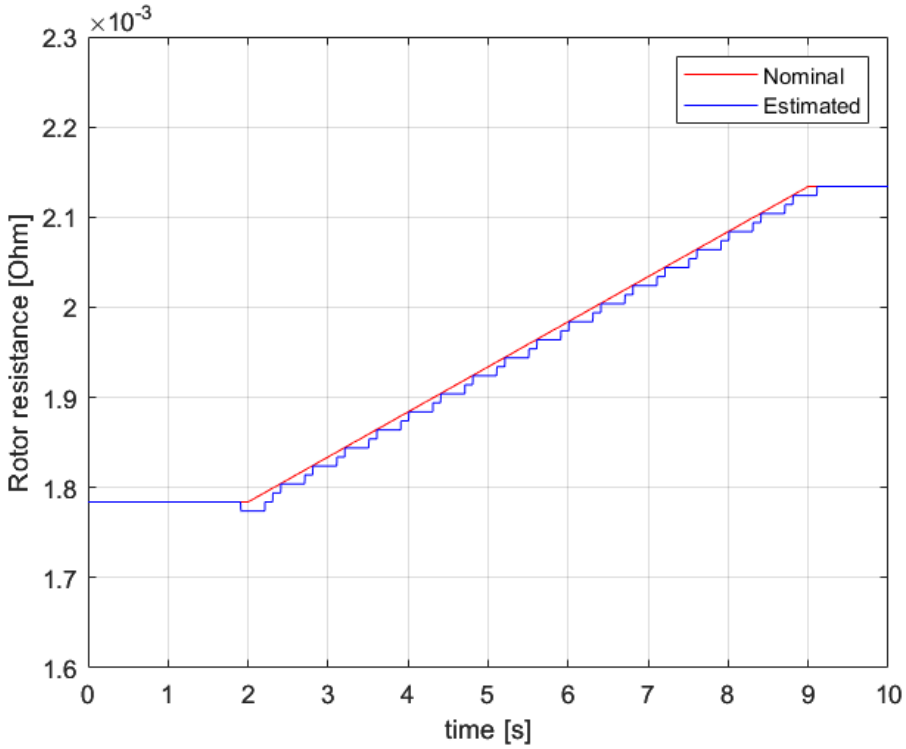

Figure 5.9: Rotor resistance estimation when steady-state is reached

Figure 5.8 depicts that after 2 seconds, the estimated value closely follows the nominal value. The staircase waveform is caused by the $\Delta\hat{R}_r$ which, as previously explained, is arbitrarily chosen. The smaller the $\Delta\hat{R}_r$ is, the closer to a continuous variation of the rotor resistance will be obtain.

Furthermore, when the rotor resistance reaches a steady-state value after rising from its nominal value as shown in Figure 5.9, the estimated value is equal to the real one.

This method does not require knowledge of the machine parameters beyond what is necessary for vector control. The technique has a low computational requirement, making it well-suited for implementation on existing vector controllers without the need for a processor upgrade.

In conclusion, both rotor resistance estimation techniques yield accurate results, positioning them as suitable choices for inclusion in the control system of an induction machine. By utilizing these estimation techniques, the performance of the IM can approach that of a PMSM, while enjoying the advantage of not relying on rare earth materials for magnets. This aspect makes the IM option more appealing from a sustainability standpoint.

5.2 Future work

Improve the MTPA algorithm used in the MRAS estimator. During this project, the MTPA algorithm was implemented taking into account only positives torques. In real cars, MTPA technique must be implemented for both positives an negatives torques. Furthermore, the algorithm should consider the following aspects to be more accurate:

1. Rotor temperature mapping.
2. Variable DC voltage.
3. Variations in magnetizing inductance and stator resistance.

Discretize the model and test it in a rig, so that afterwards may be implemented in real cars.

Better tuning of the PI speed controller. Variable bandwidth may be a good idea. When the machine is working at low speeds higher bandwidth could be used, so that the system rises quicker. On the other hand, when there is noise in the measurements, the controller becomes more unstable at high speeds and then a reduction of bandwidth could make it more stable again. This is due to the controller operating much closer to its maximum capacity, and can therefore, enter more easily in saturation which makes it unstable. Lower bandwidth will make it less likely to enter saturation. Moreover, if bandwidth is lower the demanded torque will be lower too because Kpw and Kiw will also be smaller.

With regard to the HFSI estimator, the implementation of a band pass filter (BPF) or a low pass filter (LPF) would be beneficial for this estimator. In a simulation environment there is no noise, however, in real life there will be a lot of noise, therefore, the design of a proper filter to eliminate the noise would be an improvement.

Bibliography

[1] R. Marino, S. Peresada and P. Tomei, "On-line stator and rotor resistance estimation for induction motors," in IEEE Transactions on Control Systems Technology, vol. 8, no. 3, pp. 570-579, May 2000, doi: 10.1109/87.845888.

[2] K. Akatsu and A. Kawamura, "Online rotor resistance estimation using the transient state under the speed sensorless control of induction motor," in IEEE Transactions on Power Electronics, vol. 15, no. 3, pp. 553-560, May 2000, doi: 10.1109/63.844516.

[3] S. Wade, M. W. Dunnigan, and B. W. Williams, "A new method of rotor resistance estimation for vector controlled induction machines," IEEE Trans. Ind. Electron., vol. 44, no. 2, pp. 247–257, Apr. 1997.

[4] Maiti, S., Chakraborty, C., Hori, Y., & Ta, M. C. (2008). Model reference adaptive controller-based rotor resistance and speed estimation techniques for vector controlled induction motor drive utilizing reactive power. IEEE Transactions on industrial Electronics, 55(2), 594-601.

[5] H. Bin, Q. Wenlong, and L. Haifeng, "A novel on-line rotor resistance estimation method for vector controlled induction motor drive," in Proc. Conf. Rec. IEEE IPEMC Conf., 2004, vol. 2, pp. 655–660.

[6] L. Garces, "Parameter adaption for the speed-controlled static AC drive with a squirrel-cage induction motor," IEEE Trans. Ind. Appl., vol. IA-16, no. 2, pp. 173–178, Mar./Apr. 1980.

[7] M. S. Nait Said and M. E. H. Benbouzid, "Induction motors direct field oriented control with robust on-line tuning of rotor resistance," IEEE Trans. Energy Convers., vol. 14, no. 4, pp. 1038–1042, Dec. 1999.

[8] Notes from Electric systems: Asynchronous Machine.

[9] Bose, B. K. (2002). Modern power electronics and AC drives (Vol. 123). Upper Saddle River, NJ: Prentice hall.

[10] BOLDEA, Ion; NASAR, Syed A. Electric drives. CRC press, 2016.

[11] Notes from Electric Drives.

[12] Shashank Arora, Alireza Tashakori Abkenar, Shantha Gamini Jayasinghe, Kari Tammi, Chapter 7 - Drivetrain Control System in Heavy-duty Electric Vehicle Applications, Editor(s): Shashank Arora, Alireza Tashakori Abkenar, Shantha Gamini Jayasinghe, Kari Tammi, Heavy-Duty Electric Vehicles, Butterworth-Heinemann, 2021, Pages 159-172

[13] T. Du, P. Vas, and F. Tronach, "Design and application of extended observers for joint state and parameter estimation in high-performance AC drives," Proc. Inst. Electr. Eng.—Electr. Power Appl., vol. 142, no. 2,pp. 71–78, Mar. 1995.

[14] Duran, M. J., & Fernandez, J. (2004). Lumped-parameter thermal model for induction machines. IEEE transactions on Energy Conversion, 19(4), 791-792.
[15] M. Boussak and G. A. Capolino, “Recursive least squares rotor time constant identification for vector controlled induction machine,” Electr. Mach. Power Syst., vol. 20, no. 2, pp. 137–147, 1992
[16] B. Karanayil, M. F. Rahman, and C. Grantham, “On-line stator and rotor resistance estimation scheme using artificial neural networks for vector controlled speed sensorless induction motor drive,” IEEE Trans. Ind. Electron., vol. 54, no. 1, pp. 167–176, Feb. 2007.
[17] M. Ta-Cao and H. Le-Huy, “Rotor resistance estimation using fuzzy logic for high performance induction motor drives,” in Proc. Conf. Rec. IEEE IECON Annu. Meeting, 1998, vol. 1, pp. 303–308
[18] Baird, Christopher S. “Electromagnetism.” AccessScience, McGraw Hill, May 2019.
[19] Raymond A. Serway and John W. Jewett, "The Laws of Motion", Physics for scientists and Engineers with modern physics, 9th ed Boston, MA, USA: Cengage Learning, 2015.
[20] Y. P. Landau, Adaptive Control: The Model Reference Approach. New York: Marcel Dekker, 1979
[21] K. -R. Cho and J. -K. Seok, "Induction Motor Temperature Estimation Based on High-Frequency Model of Rotor Bar," 2008 IEEE Industry Applications Society Annual Meeting, Edmonton, AB, Canada, 2008, pp. 1-7, doi: 10.1109/08IAS.2008.208.
[22] H. Hussain, J. Yang and G. Yang, "Harmonic and Fundamental Rotor Resistance Estimation Scheme for Multiphase Induction Motor Based on Non-sinusoidal Supply Control," in IEEE Journal of Emerging and Selected Topics in Power Electronics, vol. 10, no. 2, pp. 2052-2064, April 2022, doi: 10.1109/JESTPE.2021.3136285.

DEPARTMENT OF ELECTRICAL ENGINEERING
CHALMERS UNIVERSITY OF TECHNOLOGY
Gothenburg, Sweden
www.chalmers.se

CHALMERS
UNIVERSITY OF TECHNOLOGY